Photochemical Deposition of SnO_2 Thin Films for Hydrogen Sensor Applications

by

Ao Dengbaoleer

Thesis for Ph. D. degree of engineering

Department of Engineering Physics, Electronics and Mechanics,

Graduate School of Engineering,

Nagoya Institute of Technology,

Nagoya, Japan.

March 2013

Abstract

Room temperature hydrogen sensors based on SnO_2 thin films were fabricated and characterized. SnO_2 thin films were deposited by the drop-photochemical technique. The photochemically deposited films constitute of small particles, and the resulting high surface-to-bulk ratio is expected to enhance the number of sites for the gas reaction, which is advantageous for a low operation temperature gas sensor application.

This thesis has seven chapters. In the first chapter, we introduced a brief background on the metal oxide semiconductor sensors: importance, history, new concept and basic theory. In this chapter, we also introduced the sensor fabrication techniques including the photochemical deposition, which was used in this work.

In the second chapter, SnO_2 thin films were deposited by the drop-photochemical technique from an aqueous solution containing $SnSO_4$. The solution were dropped onto the glass substrate and irradiated with UV light of an ultra-high-pressure mercury arc-lamp. After 5 min irradiation, the substrate was washed and the new solution was dropped. The films were fabricated by repeating this process. The sample annealed at 200 °C showed high sensitivity to hydrogen at room temperature. The sample showed current increased by a factor $>10^4$ within 1 min to 5% H_2+Ar mixed gas (0.1atm). The removal of hydrogen from the ambient caused only a small decrease in the current, but the current decreased by more than three orders of magnitude almost instantly upon subsequent exposure to air.

In the third chapter, to improve the gas sensor properties further, the surface condition of SnO_2 thin films was modified by 1) changing the annealing ambient from nitrogen to oxygen, and 2) irradiating the sensor surface with the UV light of a low-pressure mercury lamp after annealing. The oxygen annealed sensor showed higher sensitivity for the high concentration hydrogen than the nitrogen annealed one, but the sensitivity for the low concentration

hydrogen was inferior. On the other hand, the sensitivity and response speed were improved by the UV irradiation. XPS study was performed in order to understand the relation between the change in the chemical states of Pd involved in the film surface and the change in the sensitivity by the oxygen annealing and UV irradiation. It was revealed that percentages of metal Pd, PdO and PdO_2 were almost the same for the all samples, and that Pd was dominantly in the metallic or elemental state.

In the fourth chapter, Sb-doped and Cu-doped SnO_2 thin films were deposited on glass substrates by the drop-photochemical technique. A solution containing $SnSO_4$ and a doping solution containing $SbCl_3$ or $CuSO_4$ were alternately dropped on the glass substrate and irradiated by the UV light. Auger electron spectroscopy measurement revealed that Sb or Cu was contained in the deposited thin films. The conduction type judged by the hot probe method was n-type for all the samples annealed at 400°C. The optical measurements revealed that the band gap was around 3.7 - 3.8 eV for the undoped and doped SnO_2 thin films. The dependence of electrical properties of the films on annealing temperature was studied. The Cu-doped SnO_2 thin film showed enhanced electrical conductivity after 400°C annealing in a nitrogen atmosphere.

In the fifth chapter, Fe-doped SnO_2 thin films were deposited by the drop-photochemical method. For the Fe doping, $FeSO_4$ was mixed in the SnO_2 deposition solution, or another solution for the Fe doping was prepared separately and alternately dropped and irradiated. Auger electron spectroscopy measurement revealed that Fe was contained in the deposited thin films when the separate solution was used. The dependence of electrical properties of the films on annealing temperature was studied and compared with the previous chapter results. The resistivity of the 300 and 400°C annealed films was significantly reduced by the Fe-doping using the 2 mmol/L $FeSO_4$-mixed solution and the separate solution containing 20mmol/L $FeSO_4$.

In the sixth chapter, a highly sensitive room temperature hydrogen sensor based on doped and undoped SnO_2 films were fabricated by the drop-photochemical deposition and annealing at 400°C. The doped and undoped samples showed resistance decrease by a factor $>10^3$ for a 5% H_2+Ar mixed gas (0.1atm) at room temperature. Response of a portable hydrogen detector consisting of the sample and a pocket tester was investigated. The Fe-doped sample showed higher sensitivity compared with the undoped sample to the mixed gas of the air and hydrogen.

In the seventh chapter, conclusion of this work and suggestions for future work have been introduced.

Acknowlegements

I would like to express my gratitude to all those who helped me during the doctoral research work.

First of all, I would like to extend my sincere gratitude to my supervisor, Prof. Masaya Ichimura for his instructive advice and invaluable suggestions. He has walked me through all the stages of the writing of this thesis. Without his consistent and illuminating instruction, this thesis could not have reached its present form.

All my gratitude to Prof. Takashi Egawa and Prof. Yo Ichikawa for the time they spent reading and commenting my thesis. Their ideas and suggestions have helped me to improve the thesis.

I am most grateful to Dr. Masashi Kato for his comments, advice and discussion.

I would also thank you to all the members of thin-film group for their friendship, useful discussions and technical assistance especially at the beginning of this work. Among them, I am deeply thankful to Mr. Sueyoshi, and Mr. Nakashima. I also wish to thank Mr. Moriguchi for their technical assistance concerning the XPS measurements.

I am grateful to Japan Student Services Organization (JASSO) and NGK scholarship which helped me to accomplish this work.

I should finally like to express my gratitude to my beloved family who have always been helping me out of difficulties and supporting without a word of complaint.

Abstract

Acknowledgement

Chapter 1: Introduction

Chapter 2: Properties of gas sensors based on photochemically deposited nanocrystalline SnO$_2$ films

Chapter 3: UV irradiation effects on hydrogen sensors based on SnO$_2$ thin films fabricated by the photochemical deposition

Chapter 4: Deposition and characterization of Sb and Cu doped nanocrystalline SnO$_2$ thin films fabricated by the photochemical method

Chapter 5: Deposition of Fe doped nanocrystalline SnO₂ thin films by the photochemical deposition method

Chapter 6: Fabrication of portable hydrogen sensors based on photochemically deposited SnO₂ thin films

Chapter 7: Conclusions

Chapter 1
Introduction

1.1 Hydrogen Energy

Energy supply security and global warming continue to challenge all countries around the world in terms of both the global economy and the planetary environment. Renewable energy technologies are being explored to meet the challenges of energy security and climate change, as well as to boost regional and national economic development. Hydrogen is an energy "carrier" with great potential to increase energy security and to reduce greenhouse gas (GHG) emissions.

Hydrogen is the simplest element. An atom of hydrogen consists of only one proton and one electron. It's also the most plentiful element in the universe. Despite its simplicity and abundance, hydrogen doesn't occur naturally as a gas on the Earth - it's always combined with other elements. Water, for example, is a combination of hydrogen and oxygen (H_2O). A fuel cell is a device that converts the chemical energy from a fuel into electricity through a chemical reaction with oxygen or another oxidizing agent. Hydrogen is the most common fuel used in fuel cells and is also the least harmful to the environment. The only byproducts of the oxidation reaction between hydrogen and oxygen are electricity, heat and water vapor. In many cases, this heat can be recaptured for use in industrial or residential applications, greatly increasing the system's total efficiency.

In the future, hydrogen can be an important electrical energy carrier. An energy carrier moves and delivers energy in a usable form to consumers. Renewable energy sources, like the sun and wind, can't produce energy all the time. But they could produce electric energy and hydrogen, which can be stored until it's needed. Hydrogen can also be transported (like electricity) to locations where it is needed.

1.2 Metal oxide Semiconductor sensors

1.2.1 Introduction

Gas sensors for detecting the atmospheric environment must be able to operate stably under deleterious conditions, including chemical and/or thermal attack. It means that long-term stability of gas sensor's output signal is one of the most important factors determining the practical use of such device. Of all the gas sensing solid state materials, metal oxides were one of the first considered and are still the most widely used gas sensing materials. This choice is partially due to the chemical stability of oxides at the operation conditions of gas sensors, high sensitivity and fast response. Beside, owing to the advantages of low cost, small size, simple structure, easiness to integrate, and no need of reference electrode, special attention is paid to the semiconducting metal-oxide gas sensors all over the world.

Since 1962 it has been known that absorption or desorption of a gas on the surface of a metal oxide changes the conductivity of the material, this phenomenon being first demonstrated using ZnO thin film layers by Seiyama et al [1] and porous SnO_2 [2] ceramics by Taguchi. After that, doping small amounts of noble metals (such as Pt and Pd) to these oxides were shown to be effective in improving their sensing properties [3]. At present, various metal oxide semiconductors including SnO_2, WO_{3-x}, ZnO, MoO_3, and TiO_2, have been widely used for sensing various kinds of reducing or oxidizing gases [4-16].

In recent years, with the focus on environmental and energy problems increase, development of the gas sensor which detects the environmental pollution gas, volatile organic compounds, and hydrogen and ethanol is progressing. Especially, the hydrogen used for fuel cell material is expected as next-generation energy. However, hydrogen is difficult to store and transport because it is extremely flammable, explosive, and can easily leak from gas-handling equipment if carelessly handled. Consequently, the detection of hydrogen leakage has become an issue of crucial importance. Resistive gas sensors based on oxide

semiconductors such as SnO_2 have been widely used because of their high stability and sensitivity, but usual resistive gas sensors need to be heated up to 300°C or above to enhance the sensitivity and response speed. In addition heated sensors have limited use in applications such as flammable gas detection due to excessive power consumption, possible hazards and the complex circuitry required to maintain accurate temperature control. For these reasons the need for the external heating limits the miniaturization of some current sensor types and the development of portable instrumentation.

The new concept of nanostructure as applied to the semiconducting metal oxide gas sensors does not only improve the sensing properties in terms of sensitivity and response time, but also effectively reduces the operating temperature, and improves integrated circuit density for hybrid-array gas sensors. It has also given rise to the accelerated development in semiconducting metal oxide gas sensors with low power, small size, and relatively low cost.

1.2.2 Basic theory

Metal oxide Semiconductor sensors detect gases via the variations in their conductivity (or resistivity). The target gas interacts with the surface of the metal oxide film (generally through surface adsorbed oxygen ions), which results in a change in charge carrier concentration of the material. This change in charge carrier concentration serves to alter the conductivity (or resistivity,) of the material. An n-type semiconductor is one where the majority charge carriers are electrons, and upon interaction with a reducing gas an increase in conductivity occurs. Conversely, an oxidizing gas serves to deplete the sensing layer of charge carrying electrons, resulting in a decrease in conductivity. A p-type semiconductor is a material that conducts with positive holes being the majority charge carriers; hence, the opposite effects are observed with the material and showing an increase in conductivity in the presence of an oxidizing gas (where the gas has increased the number of positive holes). A resistance increase with a reducing gas is observed, where the negative charge introduced in to the material reduces the positive (hole) charge carrier concentration. A summary of the response is provided in Table

1.1.

Table 1.1 Sign of resistance change (increase or decrease) to change in gas atmosphere.

Classification	Oxidizing gases	Reducing gases
n-type	Resistance increase	Resistance decrease
p-type	Resistance decrease	Resistance increase

The detail process for the n-type metal oxide semiconductor sensors is that the adsorbed oxygen forms a spaces-charge region on the surfaces of the metal-oxide grains; it results in an electron transfer from the grain surfaces to the adsorbates as follows:

$$O_2^{(g)} + 2e^- = 2O^-_{ads}$$
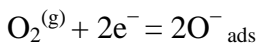
The depth of this space-charge layer (L) is a function of the surface coverage of oxygen adsorbates and intrinsic electron concentration in the bulk. Before the sensor is exposed to reducing gases, the resistance of an n-type semiconducting metal oxide gas sensor in air is therefore high, due to the development of a potential barrier to electronic conduction at each grain boundary, as shown in Fig. 1.1. When the sensor is exposed to an atmosphere containing reducing gases at elevated temperatures, the oxygen adsorbates are consumed by the subsequent reactions, so that a lower steady-state surface coverage of the adsorbates is established. During this process, the electrons trapped by the oxygen adsorbates are returned to the oxide grains, leading to a decrease in the potential barrier height and a drop in resistance.

(a) Physical Model
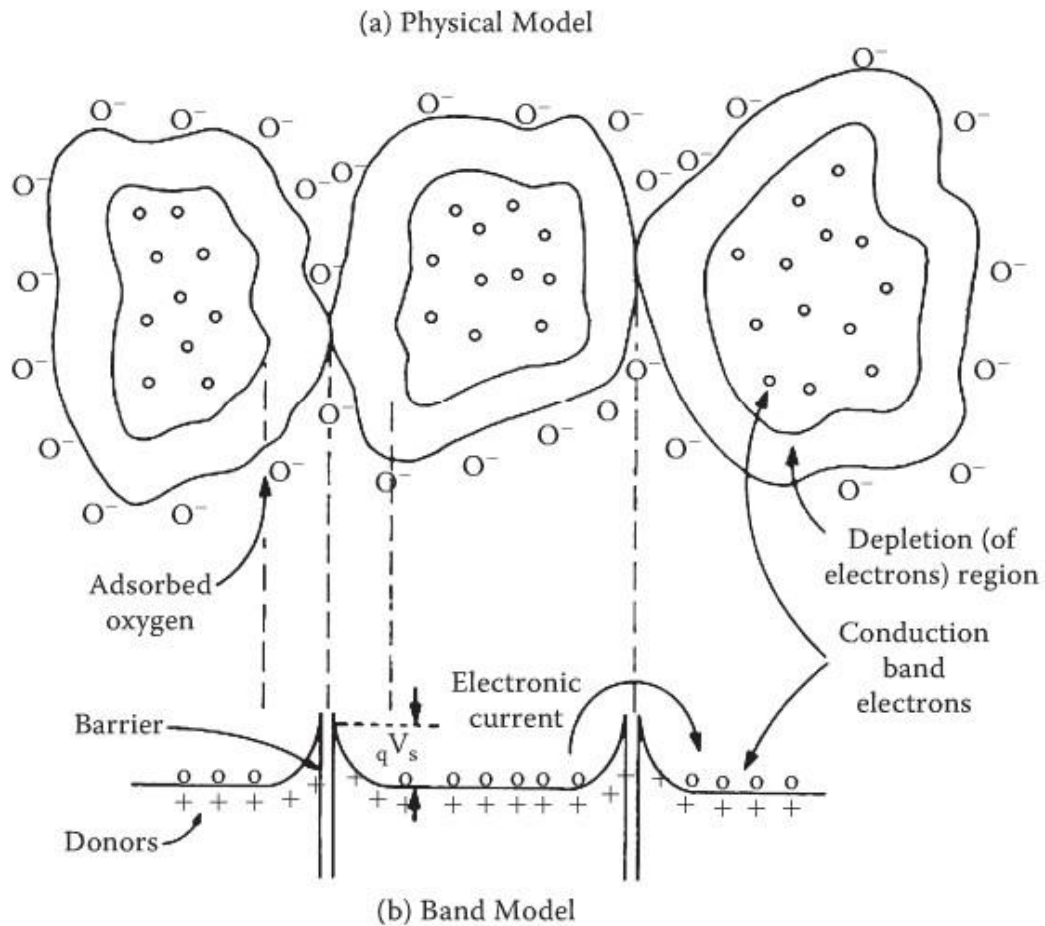
(b) Band Model

Fig .1.1 Model for adsorbate-dominated n-type semiconducting in gas sensing
(a): Physical Model. (b): Band Model.

1.3 Techniques for sensor fabrication

Many fabrication methods have been used in the production of metal oxide semiconductor sensors. Factors that must be considered when selecting the production technique include; expense (if the films are expensive, the demand will be low and will have only limited applications), purity, porosity (if the material is highly porous, the surface area available to the gas for interaction will be far higher, giving a higher sensitivity), reliability and reproducibility.

In order to lower the operating temperature of metal oxide semiconductor sensors, enhancement of surface reaction kinetics is necessary which is done by increasing available gas adsorption sites on the film surface. Nano-crystalline materials offer a solution to this problem by having a higher surface to volume ratio of the constituting particles. Nano-crystalline powders, thick and thin films of metal oxide have been synthesized by using various techniques such as spray pyrolysis [17-19], sol-gel [20-23], chemical vapor deposition (CVD) [24,25], and sputtering techniques [26-30] among others.

1.3.1 Sputtering

In sputtering process, as shown in Fig. 1.2, the substrate is placed in a vacuum chamber (discharge tube) with the source material, named a target, and an inert gas (such as argon) is introduced at low pressure. In this discharge tube a high energy voltage is given between the two electrodes creating the ionization of the argon ions. The positive argon ions move toward
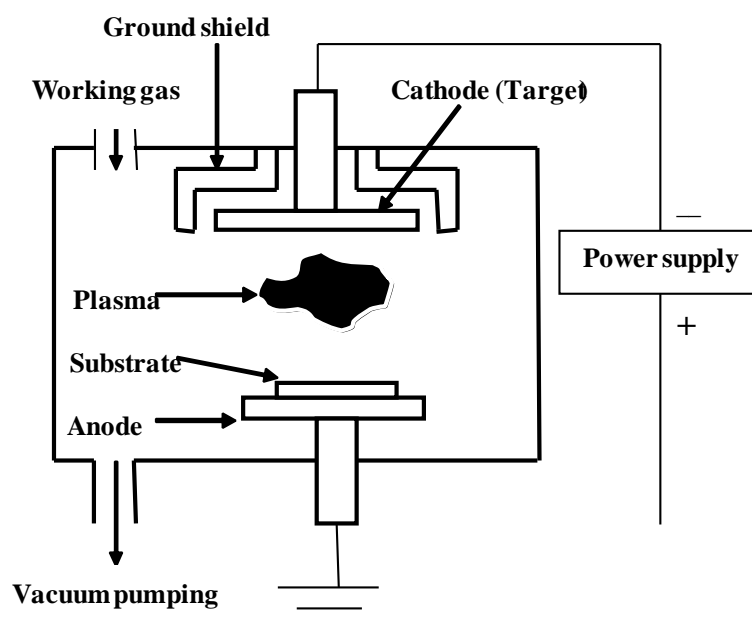

Fig. 1.2 Schematic diagram of the sputtering equipment.

the cathode with a very high momentum and hit the target. The atoms, at the target surface, get momentum from the argon ion with that momentum it comes out in a vapor form and condense on all surfaces including the substrate. The basic principle of sputtering is the same for all sputtering technologies. The differences typically relate to the manner in which the ion bombardment of the target is realized. Sputtering is performed under vacuum; on large scale this can be an expensive technique. Growth rates, around 10 nm an hour makes this technique less suitable for high throughput for industrial applications.

1.3.2 Chemical vapor deposition (CVD)

In CVD process, as shown in Fig. 1.3, the substrate is placed inside a reactor to which a number of gases are supplied. The fundamental principle of the process is that a chemical reaction takes place between the source gases. The product of that reaction is a solid material with condenses on all surfaces inside the reactor. CVD gives control over important aspects of
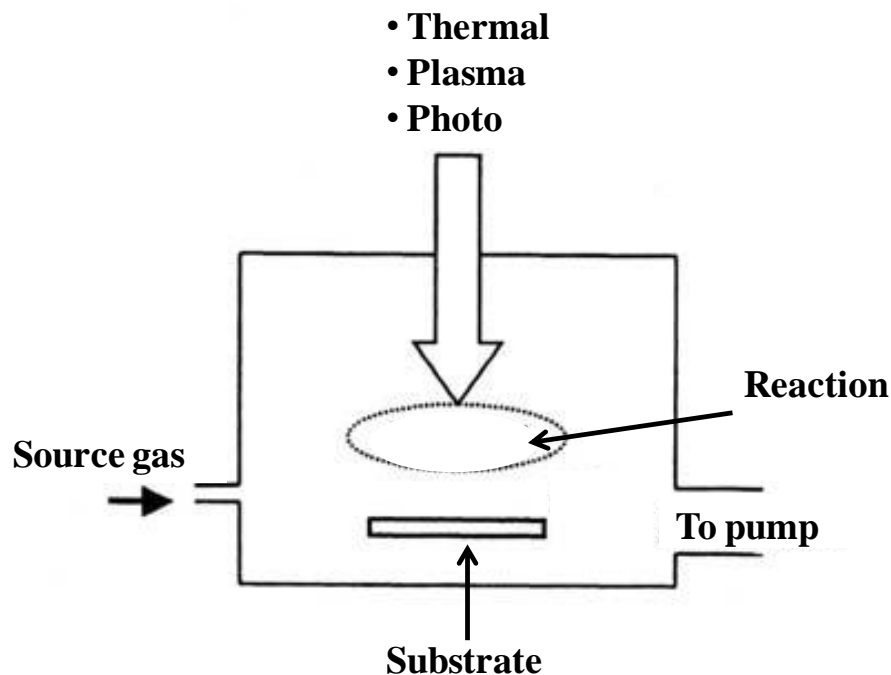
Fig. 1.3 Schematic diagram of the chemical vapor deposition.

gas sensing materials; properties such as porosity, grain size and thickness can all be well controlled using CVD.

1.3.3 Spray pyrolysis

Spray pyrolysis is a simple and an inexpensive process. As shown in Fig. 1.4, the spray gun contains a spray solution coming according to controlled manner and the air pressure gives the force and when the material get deposited on the high temperature substrate it decomposes. Unlike closed vapor deposition methods, SP does not require high quality targets and/or substrates nor does it require vacuum at any stage, which is a great advantage if the technique is to be scaled up for industrial applications. The deposition rate and the thickness of the films can be easily controlled over a wide range by changing the spray parameters.
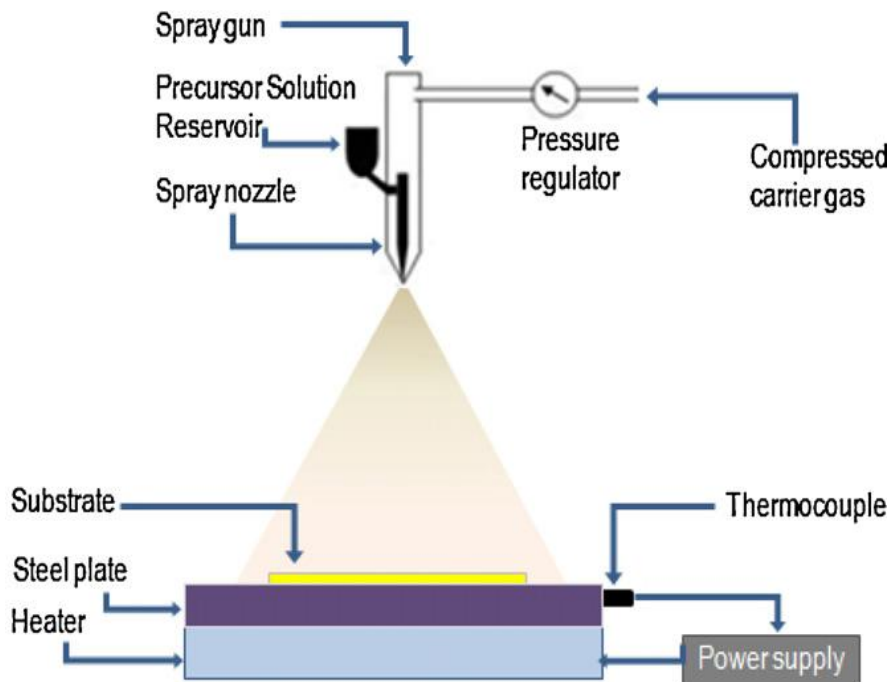

Fig. 1.4 Schematic diagram of the experimental setup for spray pyrolysis.

1.3.4 Sol-Gel deposition

The sol-gel process involves the formation of a solution (sol)- a colloidal suspension of solid particles. The sol can then undergo gelation (gel- where cross linking between particles occurs), this can give new materials with other properties. In the case of ceramic film formation, the sol then undergoes evaporation, giving a highly porous xerogel film. Upon heating, the film then forms a dense ceramic glass on the surface. The sol-gel or solution based techniques offer a very high extent of flexibility with simplicity for tailoring crystallite size and modifying the material properties.

1.3.5 Photochemical deposition

1.3.5.1 Background

A novel technique called photochemical deposition (PCD), recently has been developed to deposited compound semiconductor and a variety metals, metal oxides [31-34], sulfides [35-37] and selenides [38,39] thin film from an aqueous solution using UV light, and can be carried out at ambient temperature, from simple precursor compounds.

At the same time, some authors developed an alternative method using condensed phase precursors for the photo deposition of conducting materials in the form of films [31] or spots [32]. The technique uses UV light source to efficiently break molecular bonds, generate a new species, and induce its rapid deposition in the illuminated area [34]. On the other hand, controlled localized laser deposition of high resolution metals lines was, for example, used to repair photo mask and form interconnects in integrated circuits. That is why this technique represents now a day a well established approach for direct writing on surfaces without mask-based photolithography [40].

1.3.5.2 Process of PCD

(1) Ordinary PCD

Photochemical deposition (PCD) method involves direct irradiation of precursor bath with ultraviolet light. In PCD, the energy is absorbed by the precursor species. The absorbed photon may promote electrons to excited states (Fig. 1.5). If UV or visible wavelengths are used, the ground state energy is increased by single-or multi-photon absorption process. The simplicity of the method allows the deposition of very thin films depending on the reaction conditions and the substrates, which are not affected by the UV light. For this reason, photochemical deposition gains attention in the field of thin film technology.
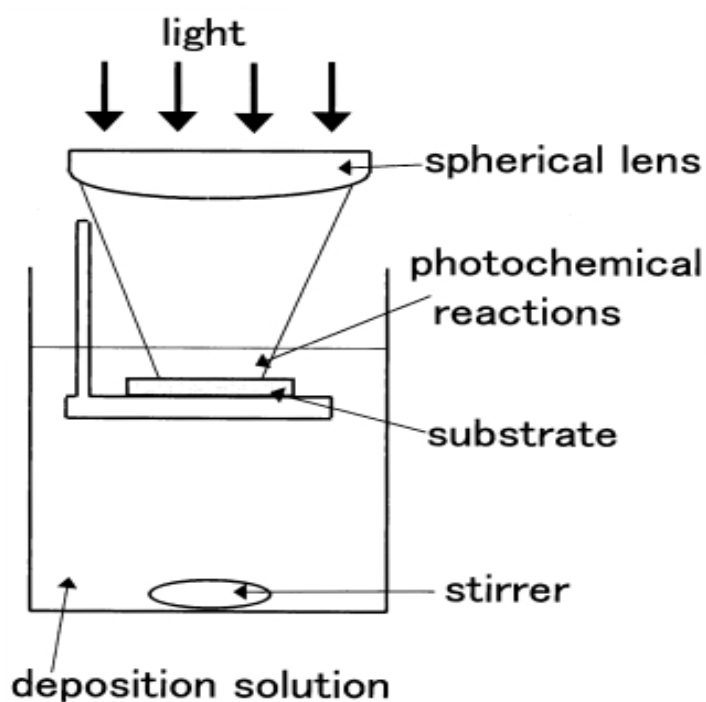

Fig. 1.5 Schematic diagram of the photochemical deposition apparatus.

(2)Drop-PCD method

In the ordinary PCD method, a thin film is deposited by irradiation on a substrate immersed in a solution. Various sulfides and selenides have been deposited by PCD. However, when this method is applied to SnO_2 deposition [41], it has the following problems: 1) the reaction is so vigorous that skims are sometimes formed on the solution surface; 2) adhesion of the film to the substrate is not good. Thus, we adopted the drop-PCD method shown in Fig. 1.6. In this method, the films are deposited by dropping a small amount of the solution (about 0.1mL over an area of 10mm) onto the glass substrate, irradiating the UV light, and repeating this process several times. No skim is formed, and reproducibility is better than for the ordinary PCD method. The substrate is a glass sheet, and the light source is an ultrahigh-pressure mercury arc lamp of 500 W. The light was focused onto an area of about 10 mmφ through a spherical lens. For SnO_2 thin films deposition, the irradiation time was fixed to 5 min, and the substrate was washed with deionized water and dried before dropping the new solution. Thin films were fabricated by repeating this process 10 times.
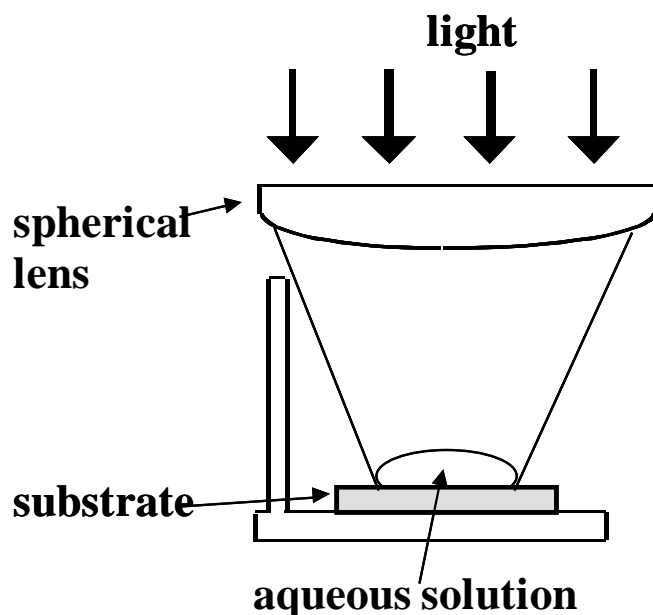

Fig. 1.6 Schematic diagram of the drop-photochemical deposition apparatus.

1.3.5.3 Advantages and disadvantages of PCD technique

The PCD technique is simple, cheap, better controllability and is capable for large area deposition. PCD offers several advantages, which includes low-temperature selected area deposition, freedom of substrate selection, and reaction controlled by optical modulation. It has also many other advantages: the method can be applied to a very broad range of precursors and the production is very easy since experiments can be performed in simple homemade tight cell.

Additionally, in the drop-PCD technique, the compound is synthesized in the solution by a photochemical reaction, and thus compound particles are expected to be formed in the solution and then deposited on the substrate. Therefore, the films constitute of small particles, and the resulting high surface-to-bulk ratio is expected to enhance the number of sites for the gas reaction, which is advantageous for a low operation temperature gas sensor application.

The problems associated with PCD are low deposition rate and the fact that the substrate position affects the deposited film thickness although it is difficult to control this position precisely [42].

1.4 Catalyst for gas sensor

1.4.1 Introduction

It is now well known that addition of small amounts of noble metals such as Pd and Pt to the elements can promote not only gas sensitivity but also the rate of response [3, 43-46]. Such promoting effects are undoubtedly related to the catalytic activities of the metals for the oxidation of reduction gases. Therefore, addition of the catalyst has played the important role for the room temperature operation gas sensor.

It is widely believed that metal catalyst enhances reducing gas sensing of metal oxide via spillover mechanism. The term spillover refers to the process illustrated in Fig. 1.7. The metal catalysts dissociates the molecule, and then the atoms can 'spillover' onto the surface of the grains of the sensor material. The reactants are first adsorbed on to the surface of additive particles and then migrate to the oxide surface to react there with surface oxygen species, resulting in affecting the surface conductivity.
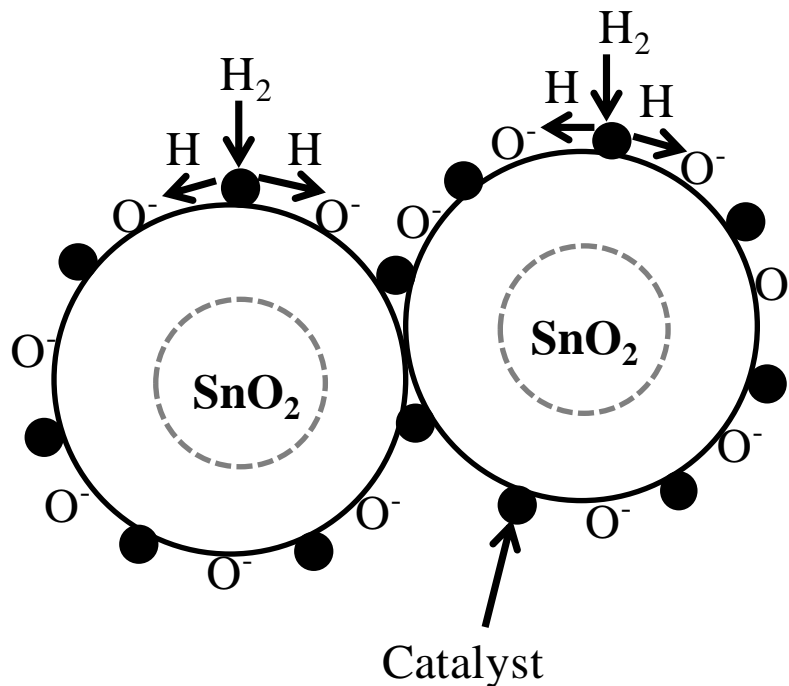
Fig. 1.7 Schematic of spillover mechanism.

1.4.2 Catalyst (Pd) doping by Photo-irradiation

To fabricate high sensitivity room temperature hydrogen sensor, we doped Pd, which, as described above, acts as a catalyst for hydrogen molecule decomposition. We developed a novel method of Pd-doping of the film, i.e., photochemical doping [47]. As shown in Fig. 1.6, a 2mmol/L $PdCl_2$ solution was dropped onto the sensing film surface and then irradiated with

the UV light for 5 min. After that, it was washed with deionized water. We expect that Pd dominantly exists as elemental or metallic state on the film surface by photochemical doping. Therefore, it will be able to effectively decompose hydrogen and lead to high sensitivity.

1.5 Objectives of this work

The main objective of this thesis is to fabricate a high sensitivity room-temperature hydrogen sensor based on photochemically deposited SnO_2 thin films. Moreover, it is also an aim of this thesis to develop a portable gas sensor with low power and low cost.

1.6 Preview of the thesis

The thesis is arranged as follows:

Chapter 2 presents the fabrication and characterization of room temperature hydrogen sensors based on SnO_2 films. The sample annealed at 200°C showed current increase by a factor $>10^4$ within 1 min for 5% H_2+Ar mixed gas (0.1atm) hydrogen at room temperature. The effects of oxygen and air on the sensor response and recovery have also been characterized.

Chapter 3 shows a detailed study for the effect of UV irradiation on SnO_2 thin films hydrogen sensor. The 200°C annealed samples were irradiated with UV light using a low-pressure mercury lamp in vacuum and in air for one hour. The sensitivity and response speed were further improved by UV irradiation.

Chapter 4 presents the photochemical deposition and characterization of Sb and Cu doped SnO_2 thin films on the glass. The Auger electron spectroscopy measurement revealed that Sb or Cu was contained in the deposited thin films. The deposited films showed good optical transmission and the band gap obtained is 3.7 - 3.8 eV. The resistivity of the 400°C annealed

films is significantly lower for the Cu-doped film than for the undoped and Sb-doped films.

Chapter 5 presents the photochemical deposition and characterization of Fe-doped SnO_2 thin films on glass substrates. The dependence of electrical properties of the films on annealing temperature was studied. The Fe-doped SnO_2 thin films deposited with 2 mmol/L $FeSO_4$-mixed solution or the separate solution containing 20mmol/L $FeSO_4$ showed enhanced electrical conductivity after 300 and 400°C annealing in a nitrogen atmosphere.

Chapter 6 presents the fabrication and characterization of room temperature hydrogen sensors based on doped and undoped SnO_2 films. The films were annealed at 400°C. The doped and undoped samples showed resistance decrease by a factor $>10^3$ for a 5% H_2+Ar mixed gas (0.1atm) at room temperature. Response of a portable hydrogen detector consisting of the sample and a pocket tester was investigated. The Fe-doped sample showed higher sensitivity to hydrogen compared with the undoped sample.

Chapter 7 presents a conclusion and suggestions for the future work.

References

[1] T. Seiyama, A. Kato, K.Fujiishi, and M. Nagatani, Anal. Chem. 34 (1962) 1502.

[2] N. Taguchi, Published patent application in Japan, S37-47677, October (1962).

[3] P.J. Shaver, Appl. Phys. Lett. 11(1967) 255.

[4] S.G. Ansari, P, Boroojerdian, S.R. Sainkar, R.N. Karekar, R.C. Aiyer, and S.K. Kulkarni, Thin Solid Films 295 (1997) 271.

[5] F. Berger, M. Fromm, A. Chambaudet, and R. Planade, Sens. Actuators B 45 (1997) 175.

[6] G.–J. Li, and S.kawi, Mater. Lett. 34 (1998) 99.

[7] V. Jayaraman, K.I. Gnanasekar, E. Prabhu, T. Gnanasekaran, and G. Periaswami, Sens. Actuators B 55 (1999) 147.

[8] S. Shukla, S. Seal, L. Ludwig, and C. Parish, Sens. Actuators B 97 (2004) 256.

[9] M. Akiyama, J. Tamaki, N. Miura, and N. Yamazoe, Chem. Lett. 9 (1991) 1611.

[10] M. Penza, C.Martucci, and G.Cassano, Sens. Actuators B 50 (1998) 52.

[11] Y.K. Chung, M.H. Kim, W.S. Um, H.S. Lee, J.K. Song, S.Ch. Choi, K.M. Yi, M.J. Lee, and K.W. Chung, Sens. Actuators B 60 (1999) 49.

[12] A.M. Gas'kov, and M.N. Rumyantseva, Russ. J. Appl. Chem. 74 (2001) 440.

[13] S.T. Shishiyanu, T.S. Shishiyanu, O.I. Lupan, Sens. Actuators B 107 (2005) 379.

[14] C. Imawan, H. Steffes, F. Solzbacher, and E. Obermeier, Sens. Actuators B 78 (2001) 119.

[15] S.S. Sunu, E. Prabhu, V. Jayaraman, K.I. Gnanasekar, T.K. Seshagiri, and T. Gnanasekaran, Sens. Actuators B 101 (2004) 161.

[16] F. Edelman, et al., Inst. Electron Technol. 33 (2000) 89.

[17] G Korotcenkov ,V Brinzari, J Schwank, M DiBattista, and A Vasiliev, Sens. Actuators B 77 (2001) 244

[18] V. Brinzari, G, Korotcenkov, V. Golovanov, J. Schwank, V. Lantto, and S. Saukko, Thin Solid Films 408 (2002) 51.

[19] H. Keskinen, A. Tricoli, M. Marjamaki, J.M. Makela, and S.E Pratsinis, J. Appl. Phys.

106 (2009) 084316.

[20] S. R. Davis, A. V. Chadwick, and J. D. Wright, J. Mater. Chem. 8 (1998) 2065.

[21] A. Dieguez, A. Romano-Rodriguez, and J. R. Morante, et al., Sens. Actuators B 60 (1999) 125.

[22] A. Chiorino, G. Ghiotti, and F. Prinetto, et al., Sens. Actuators B 59 (1999) 203.

[23] S.Shukla, S.Patil, and S. C. Kuiry, et al., Sens. Actuators B 96 (2003) 343.

[24] Y. Liu, W. Zhu, and O. K. Tan, et al., Mater. Sci. Eng. B 47 (1997) 171.

[25] S. Ashraf, C.S. Blackman, S.C. Naisbitt, and I.P. Parkin, Mes. Sci. Technol. 19 (2008) 025203.

[26] C.A. Papadopoulos, and J.N. Avarstsiotis, Sens. Actuators B 28 (1995) 201.

[27] E. Comini, G. Sberveglieri, and V. Guidi, Sens. Actuators B 70 (2000) 108.

[28] T. W. Kim, D. U. Lee, and Y. S. Yoon, J. Appl. Phys. 88 (2000) 3759.

[29] A. Karthigeyan, R. P. Gupta, and K. Scharnagl, et al., Sens. Actuators B 78 (2001) 69.

[30] A. S. Ryzhikov, R. B. Vasiliev, and M. N. Rumyantseva, et al., Mat Sci. Eng. B 96 (2002) 268.

[31] G.E. Buono-Core, M. Tejos, and G. Alveal, J. Mater. Sci. 35 (2000) 4873.

[32] G.E. Buono-Core, G. Cabello, J.L. Cayon, M. Tejos, and R.H. Hill, J. Chil. Chem. Soc. 50 (2005) 541.

[33] G.E. Buono-Core, M. Tejos, G. Alveal, N. Guzman, and R.H. Hill, Mater. Chem. Phys. 96 (2006) 98.

[34] G.E. Buono-Core, G. Cabello, H. Espinoza, A.H. Klahn, M. Tejos, and R.H. Hill, J. Chil. Chem. Soc. 51, N°.3 (2006) 950.

[35] F. Goto, M. Ichimura, and E. Arai, Jpn. J. Appl. Phys. 36 (1997) L1146.

[36] M. Ichimura, F. Goto, Y. Ono, and E. Arai, J. Cryst. Growth, 198-199 (1999) 308.

[37] J. Podder, R. Kobayashi, and M. Ichimura, Thin Solid Films 472 (2005) 71.

[38] M. Ichimura, K. Takeuchi, A. Nakamura, and E. Arai, Thin Solid Films 384 (2001) 157.

[39] R. Kumaresan, M. Ichimura, and E Arai, Thin Solid Films 414 (2002) 25.

[40] R. Kobayashi, N. Sato, M. Ichimura, and E. Arai, Journal of Optoelectronics and Advanced Materials 5 (2003) 893.

[41] M. Ichimura, K. Shibayama, and K. Masui, Thin Solid Films 466 (2004) 34.

[42] S. Chowdhury and M. Ichimura, Jpn. J. Appl. Phys. 49 (2010) 062302.

[43] N. Yamazoe, Sens. Actuators B 5 (1991) 7.

[44] K. H. Cha, H. C. Park, and K.H Kim, Sens. Actuators B 21 (1994) 91.

[45] H.T. Wang, B.S. Kang,; F. Ren, L.C. Tien, P.W. Sadik, D.P. Norton, S.J. Pearton, and J. Lin, Appl. Phys. A. 81 (2005) 1117.

[46] Y. Shen, T. Yamazaki, Z. Liu, C. Jin, T. Kikuta, and N. Nakatani, Thin Solid Films 516 (2008) 5111.

[47] D. Ito and M. Ichimura, Jpn. J. Appl. Phys. 45 (2006) 7094.

Chapter 2

Properties of gas sensors based on photochemically deposited nanocrystalline SnO$_2$ films

2.1 Introduction

Hydrogen sensors which can be operated at room temperature are highly demanded to realize an integrated sensor chip. Although there are several reports on resistive sensors having sensitivity to hydrogen at room-temperature [1-4], their performance is still not satisfactory to realize one-chip hydrogen gas sensors. In this chapter, we fabricate gas sensors having high sensitivity to hydrogen at room temperature based on SnO$_2$ films. The SnO$_2$ films are deposited by the PCD [5]. Basic properties of the gas sensors thus fabricated have been reported in a previous work [6]. The sensor showed 10^4-fold increase in conductivity within 1 min upon exposure to 5% H$_2$+Ar mixed gas (0.1atm) at room temperature. In the previous work, only response to hydrogen introduced into vacuum was reported. However, in the actual application, the sensors need to detect hydrogen in air. Thus, in this work, effects of oxygen and air on the sensor response are given, along with some more detailed characteristics.

2.2 Sensor fabrication

The films are deposited by the drop-PCD, as shown in Fig. 2.1 (a). A solution containing 10 mmol/L of SnSO$_4$ with its pH adjusted to about 2 by HNO$_3$ were dropped onto the glass substrate and irradiated with the UV light. The substrate is a glass sheet, and the light source is an ultrahigh-pressure mercury arc lamp of 500 W. The light was focused onto an area of about 10 mmφ through a spherical lens. The solution absorbs UV light with wavelength shorter than about 300 nm, and SnO$_2$ is formed in the solution. The irradiation time was 5min,

and the substrate was washed with water and dried before the new solution was dropped on it. Thin films were fabricated by repeating this process. The thickness of the film deposited by one cycle is about 15 nm. From X-ray diffraction, we confirmed that the deposit is crystalline with a coherent length of the order of 1 nm. After the film deposition, Au electrodes with an interdigit pattern with 0.2 mm spacing, as shown in Fig. 2.1 (b), were formed by vacuum evaporation. To enhance sensitivity to hydrogen, Pd was doped by a similar PCD technique [7]. A 2mmol/L PdCl$_2$ solution was dropped onto the SnO$_2$ film surface, and then irradiated with the UV light for 5 min. Pd is commonly employed for hydrogen sensors as a catalyst to decompose H$_2$ molecules. The samples were annealed in nitrogen ambient at various temperatures.
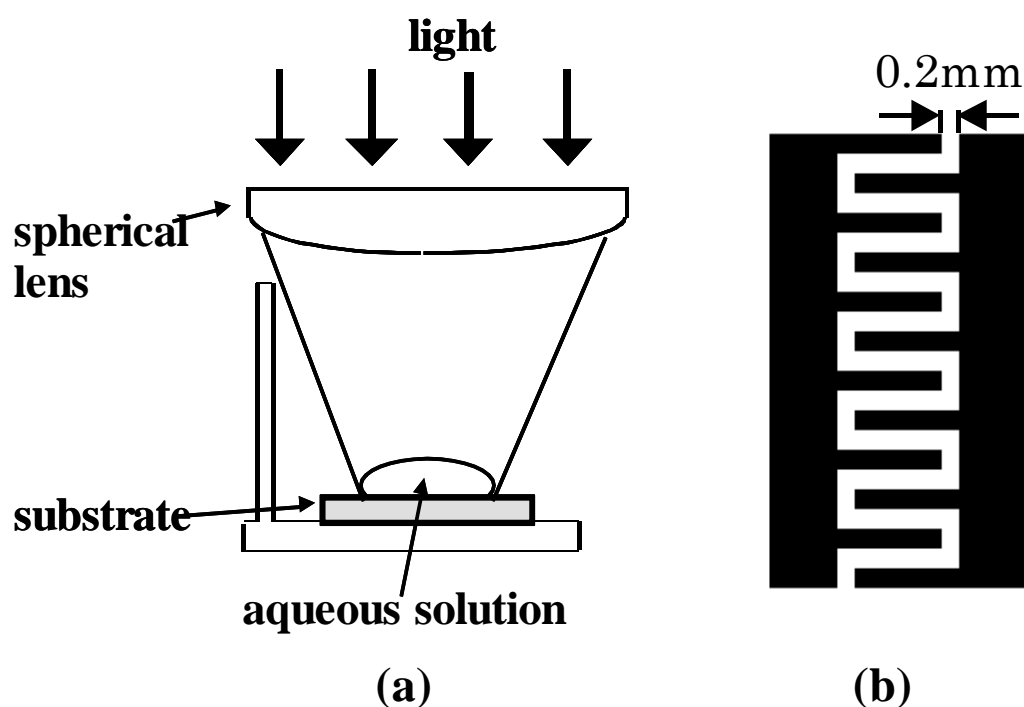

Fig. 2.1 (a): schematic of the PCD apparatus.
(b): pattern of the inter-digit electrode formed on the film.

The gas sensing properties were measured using a static test system which included a test chamber (about 18 L in volume) and an electrical-characterization workstation system.The sensor thus fabricated was set in a chamber, and current at an applied voltage of 2 V was measured at room temperature (about 300 K) first in vacuum, and then in various ambient.

2.3 Sensor characteristics

2.3.1 Thickness dependence of gas sensor properties

The thickness of film deposited by different drop-irradiation cycles is shown in Table 2.1. Atomic force micrographs of the SnO$_2$ films are shown in Fig. 2.2 (a)-(c) for different drop-irradiation cycles. For the films deposited by 5 and 10 times repetition of the drop-irradiation cycle, the surface morphology appears to consist of comparatively smooth surface and the assembled grain portion. The standard deviation roughness of the comparatively smooth portion of film with 5 and 10 times repetition of the drop-irradiation cycle are 5.35nm and 10.3nm. However, for the films deposited by 15 times repetition of the drop-irradiation cycle, the surface morphology appears to consist of the several big assembled grains, and no smooth surface portion was found.
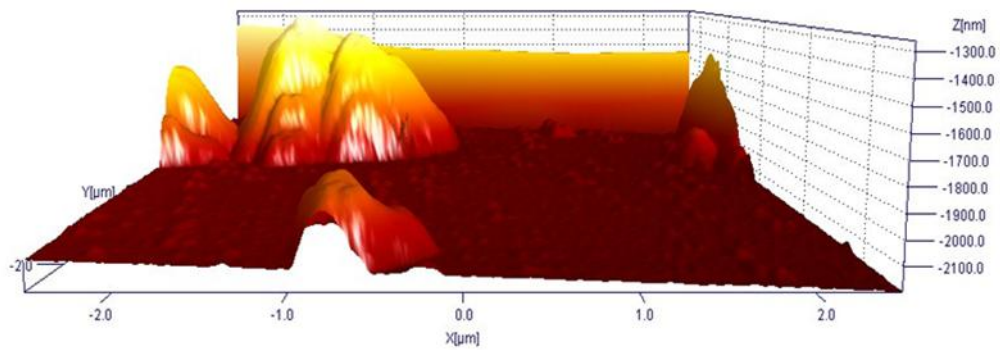
Table 2.1 Thickness dependence of drop-irradiation cycles.

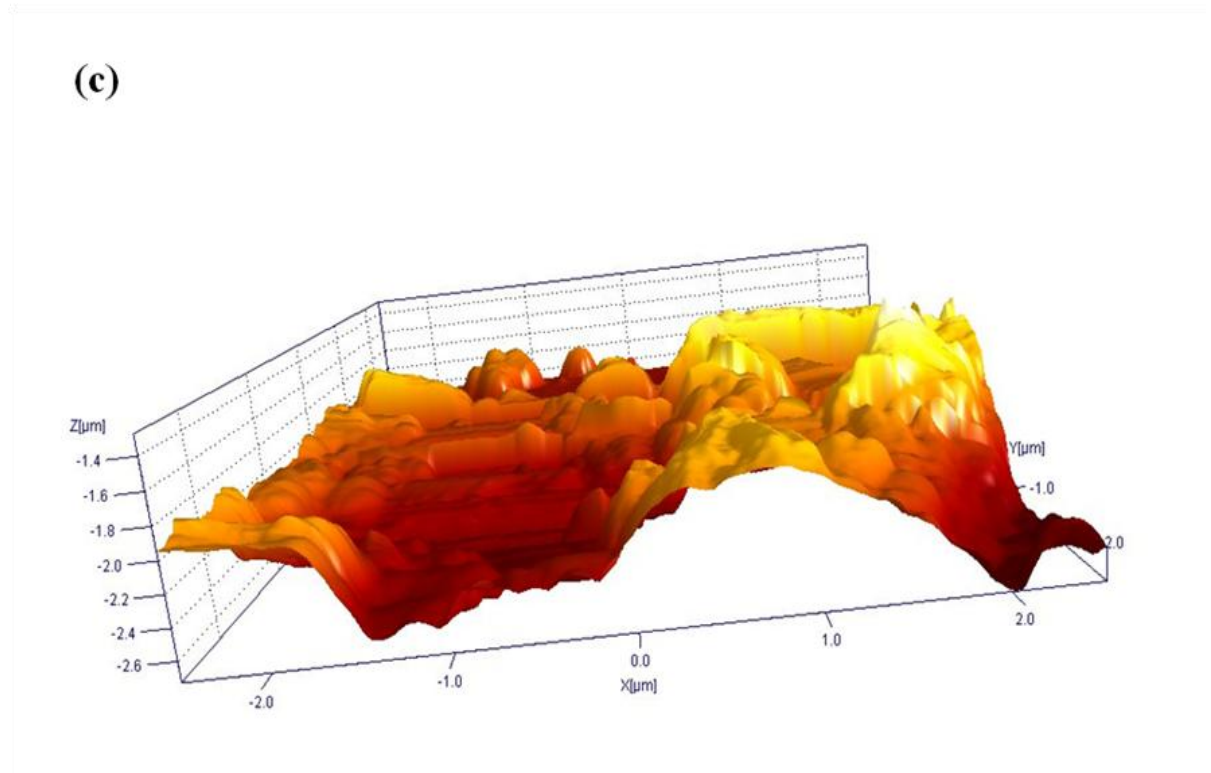| Drop-irradiation cycles（times）	Deposition time（min）	Thickness（μm）
5	25	0.075
10	50	0.125
15	75	0.3

(a)
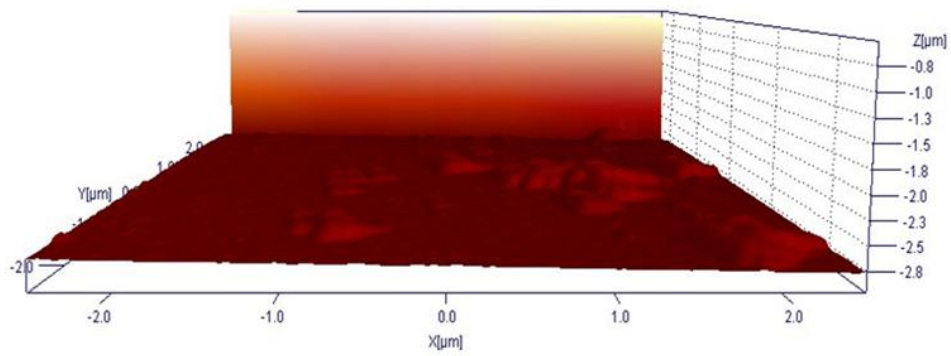
(b)

Fig. 2.2 AFM images of SnO$_2$ thin films with different drop-irradiation cycles.
(a) 5, (b) 10, (c) 15 times repetition of drop-irradiation cycles.

Figure 2.3 shows the current response to 5% H$_2$+Ar mixed gas (0.1atm) introduced into the vacuumed chamber for sensors with different film thickness. All the samples were annealed at 300 °C. For the film deposited by 5 times repetition of the drop-irradiation cycle, the current did not increase with hydrogen introduction. It seems that the current path was not formed sufficiently for this sample. Thus the current is so small that we failed to measure the response. In fact, the current of the order of 10^{-11} A would be leakage current of our measurement system, not the actual sample current. For the repetition cycles of 10 times, current increase by a factor of about 10^4 was observed upon exposure to hydrogen. When the repetition was increased to 15 times, the initial current in vacuum was large, and the increase upon exposure to hydrogen was relatively small. Those results could be explained considering that the response to hydrogen is controlled by the Schottky barrier at the boundary between the grains [8]. Initially there are negative charges due to adsorbed oxygen at the boundary between

grains, and thus the barrier height is large. Hydrogen removes the oxygen at the boundary, and reduces the barrier height. The charge density and thus the barrier height change with time exponentially, and the current depends on the barrier height exponentially. Therefore, the transient response can be fitted by a double-exponential function of time [6]. For this mechanism to be effective, the film should be composed of small grains. If the grains grow and coalesce fully, the effect of the grain boundary diminishes. The film deposited by the 10 times repetition of the drop-irradiation cycle is composed of mainly small grains with microscopic surface roughness as shown in Fig. 2.2 (b), and thus shows high sensitivity to hydrogen. By the repetition of deposition cycles 15 times, the film would become continuous as shown in Fig. 2.2 (c) and thus showed high initial current and low sensitivity to hydrogen. On the basis of the above results, the repetition time was fixed at 10.
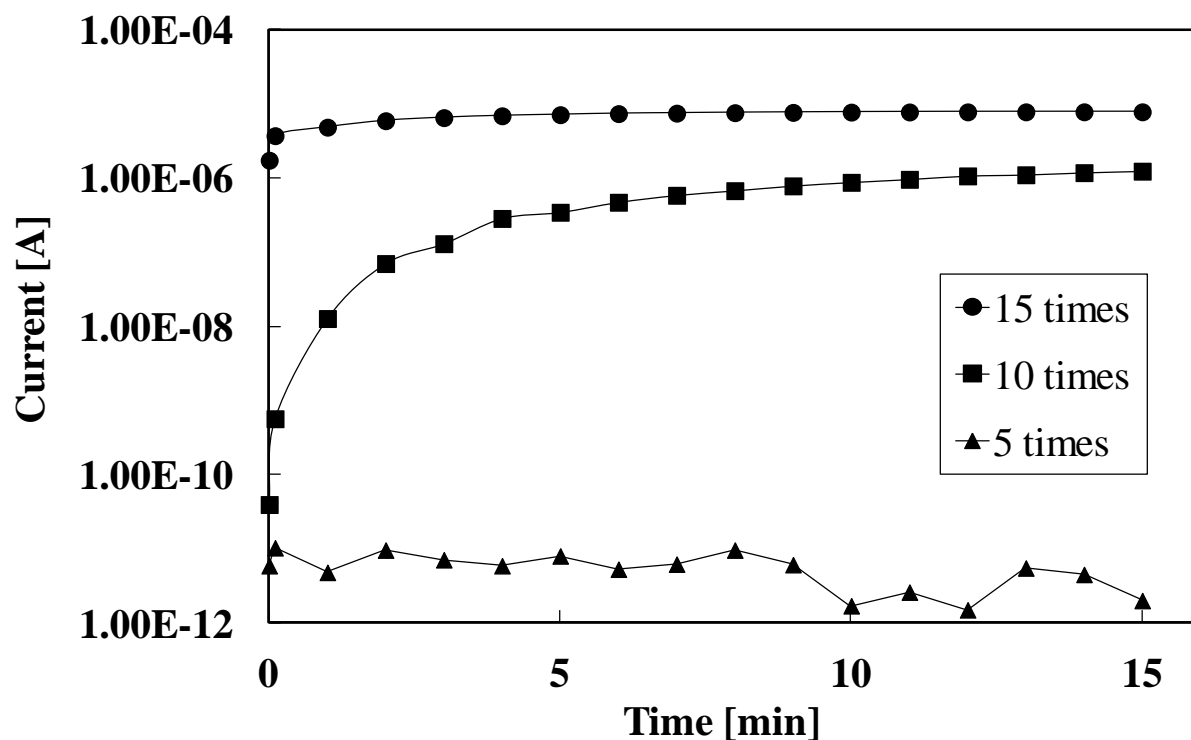

Fig. 2.3 Response to the 5% H$_2$+Ar mixed gas (0.1atm) for the samples with different thickness (different numbers of deposition cycles).

2.3.2 Effect of annealing temperature on gas sensing properties

Figure 2.4 shows the response to 5% H$_2$+Ar mixed gas (0.1atm) for the samples annealed at various temperatures [6]. For the 200-400 °C annealing, the increase of the order of 10^4 was observed. The response is most quick for the 200 °C annealed sample: the current increased more than 10^4 times and saturated within 1 min. The initial current in vacuum is larger for the higher temperature annealed sample. For the 450 °C annealed sample, the current in vacuum is large compared with the other samples, and the increase after the exposure to hydrogen is relatively small. As noted above, the as-deposited films are composed of small particles and thus have a large surface/volume ratio. The particles will coalesce and larger particles will be formed with increase in the annealing temperature. Then, conductivity in vacuum increases, and the sensitivity decreases. For the as-deposited sample, the sensor current is so small that it cannot be measured by our system due to the leakage current. To confirm the structural change by the annealing, we observed the surfaces of the films by scanning electron microscope (SEM). Figure 2.5 shows the SEM photo for the as-deposited film. The substrate surface is covered with a uniform thin layer, and there are particles of size of the order of μm on it, but detailed structure or morphology of the layer cannot be seen because of the insufficient resolution of our SEM. We observed the film surfaces after the annealing but did not confirm change in the morphology with annealing. Microscope observation with a higher resolution is necessary to prove the structural change by the annealing. We also performed annealing in oxygen and observed similar change in sensitivity with annealing temperature. Thus the annealing effects would be mainly due to structural change and not due to chemical or compositional change. Figure 2.6 shows the response to 0.05% H$_2$+Ar mixed gas (0.1atm) for the sample annealed at 200 °C. The response is slower than for 5% H$_2$+Ar mixed gas (0.1atm), but the current increase is about 10^4 fold even for such a low concentration of hydrogen.
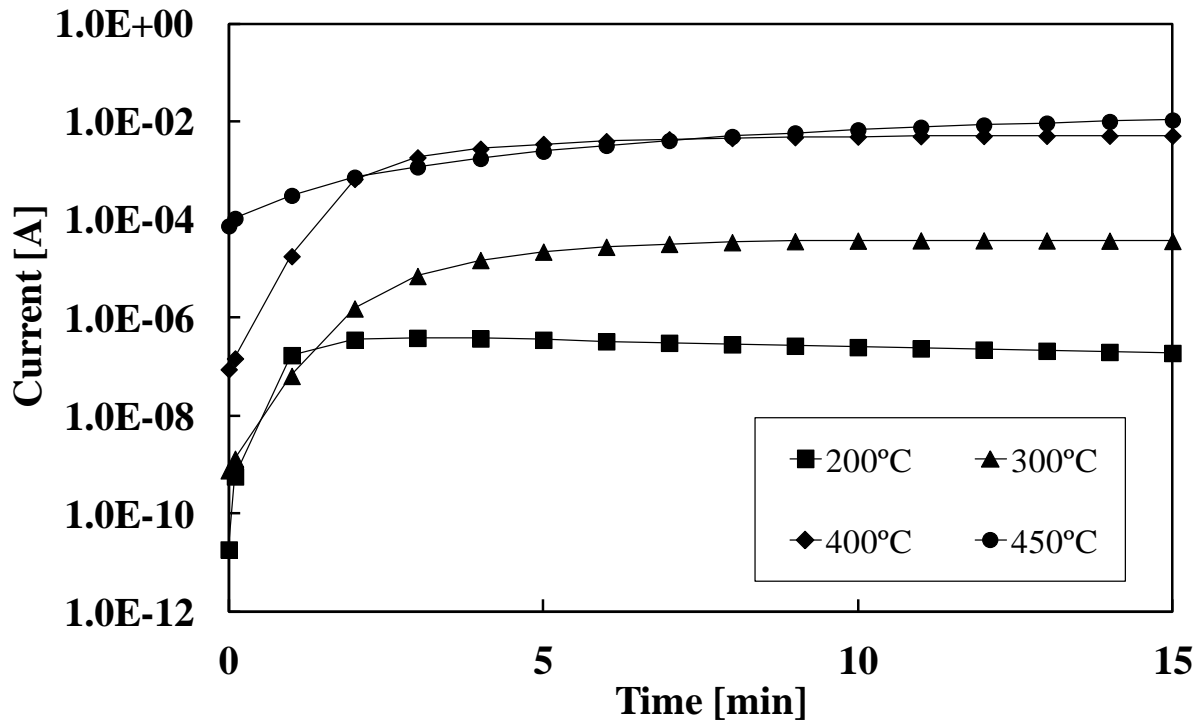
Fig. 2.4 Response to the 5% H$_2$+Ar mixed gas (0.1atm) for the samples annealed at different temperatures.
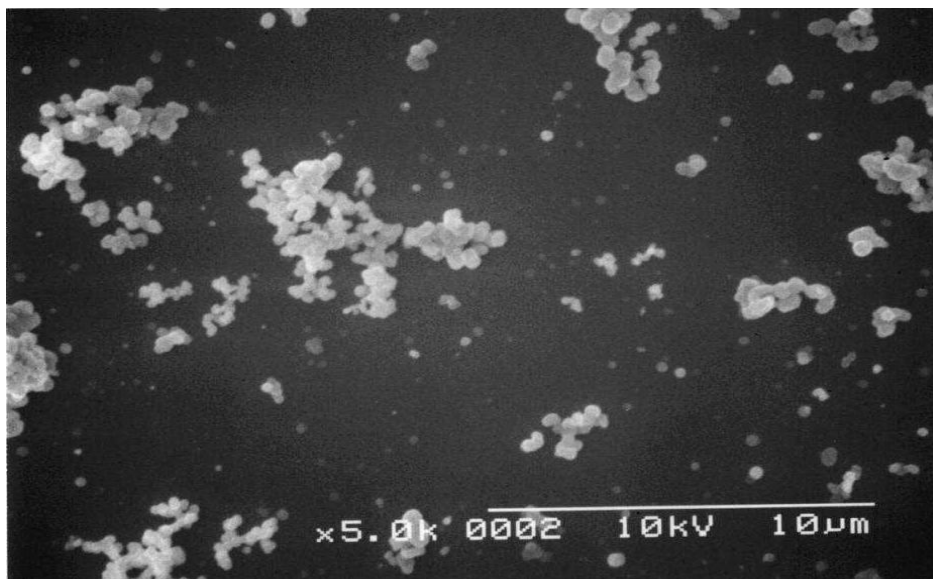

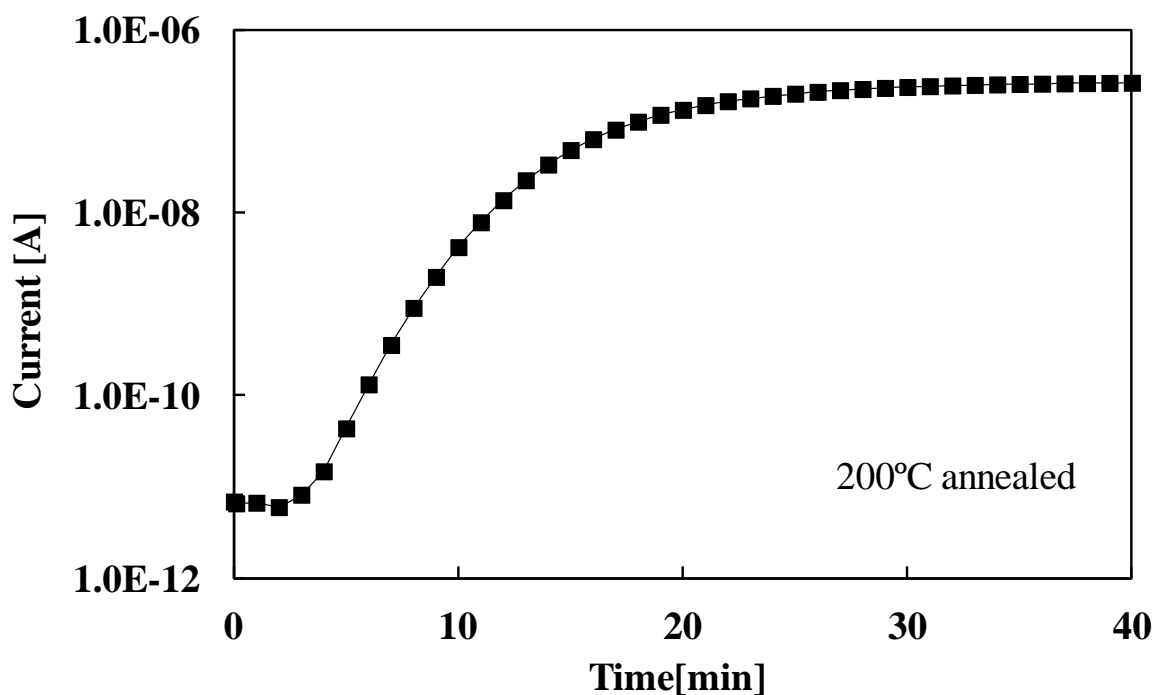**Fig. 2.5 SEM photograph of the SnO$_2$ film for the sample without annealing.**

Fig. 2.6 Response to the 0.05% H$_2$+Ar mixed gas (0.1atm) for the samples annealed at 200ºC.

2.3.3 Effect of oxygen and air on the sensor properties

Since the sensor needs to detect hydrogen in air in the actual application, we investigate effects of oxygen and air on the sensor response. Figure 2.7 shows the response to the mixed ambient. The sample was annealed at 200 °C. For the data labeled "hydrogen + oxygen", 0.2 atm oxygen was first introduced into the vacuumed chamber, and then 5% H$_2$+Ar mixed gas (0.1atm) was introduced at t=0. Similarly, for the data labeled "hydrogen + air", 0.8 atm air was first introduced and then hydrogen was introduced. Since the percentage of oxygen in air is about 20 %, oxygen content is nearly the same for both the cases. The relative humidity of air was 50−60%. As shown in the figure, the saturation value of the current became lower by about one order of magnitude with oxygen in the ambient, but the current increase was still more than 10^3 fold. For the "hydrogen + oxygen" case, the response speed was almost the same as in the hydrogen-only case, but the response was significantly slower for the
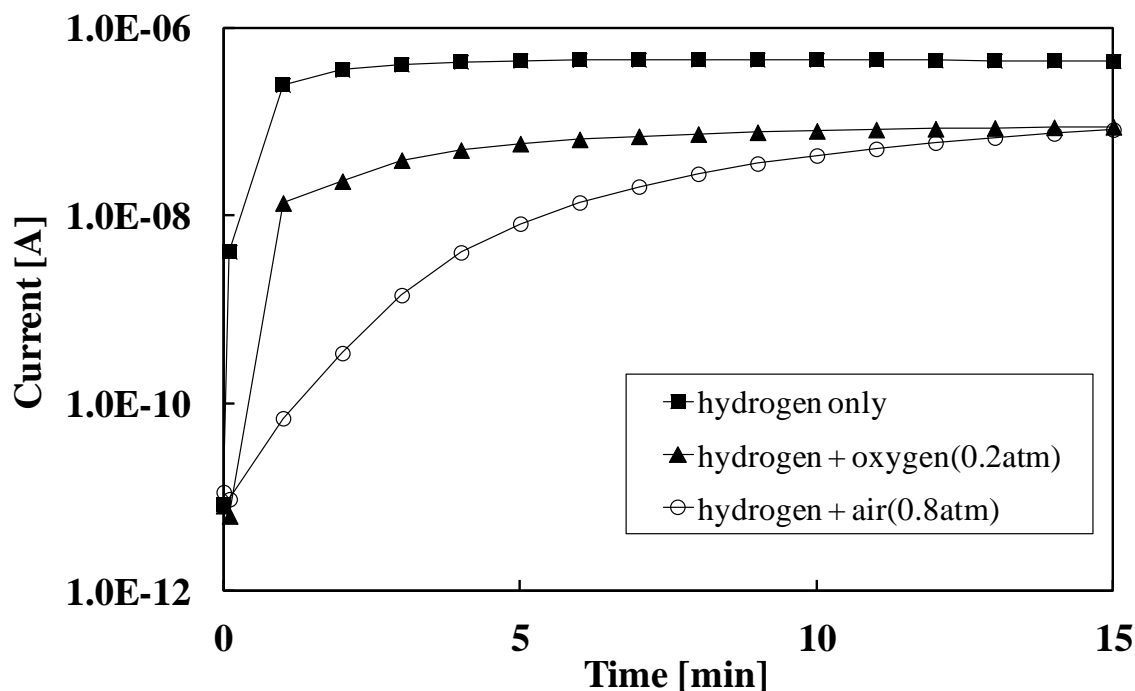
"hydrogen + air" case.

Fig. 2.7 Effects of oxygen and air on the sensor response to 5% H$_2$+Ar mixed gas. (0.1atm).

The recovery characteristics are also important characteristics of a gas sensor. The sensor current which is increased with introduction of hydrogen should decrease when hydrogen is removed. Figure 2.8 shows the recovery characteristics of the sample annealed at 200 °C. The current first increased upon exposure to 5% H$_2$+Ar mixed gas (0.1atm). Then the chamber was vacuumed. The observed decrease in current was not large, about 40% within 1 min. Then oxygen (20%) + nitrogen (80%) or air was introduced up to a pressure of 0.8 atm. When air was introduced, the current decreased by more than three order of magnitude almost instantly. On the other hand, upon exposure to oxygen + nitrogen, the decrease in current is much slower.

The results shown in Figs. 2.7 and 2.8 indicate that water vapour in air has significant effects on the sensor response. As noted above, the sensor current is thought to be controlled

by negative fixed charge due to absorbed oxygen at the grain boundary. The absorption of oxygen can be expressed as

$$O_2 + 2e- = 2O^- \qquad (1)$$

where O^- is the negatively charged oxygen atom at the surface or grain boundary, and e^- a conduction electron. Upon exposure to hydrogen, the fixed charge will be removed by the following reaction.

$$H_2 + O^- = H_2O + e^- \qquad (2)$$
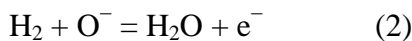
An increase in H_2O content in the ambient should make the above reaction proceed to the left-hand side. Thus both O_2 and H_2O can increase the amount of O^-, thereby decreasing the sensor current, or slowing down the current increase upon the exposure to hydrogen. The results shown in Figs. 2.7 and 2.8 show that the O^- formation by reaction (2) is much more quick and efficient than reaction (1).
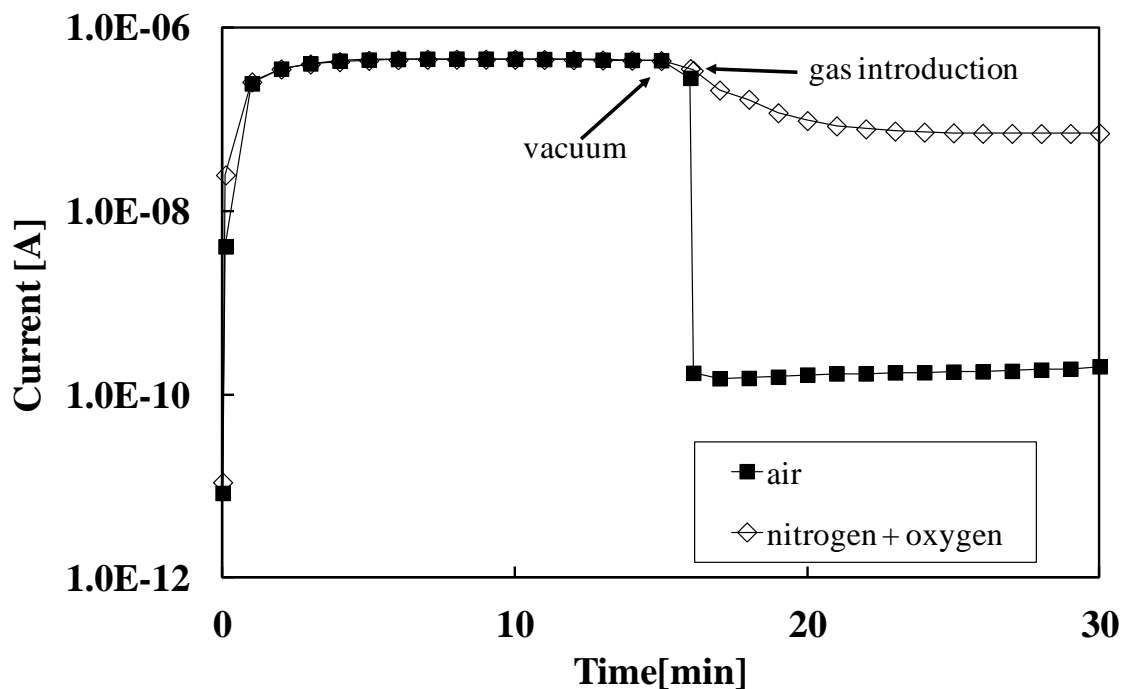

Fig. 2.8 Recovery (current decrease) after exposure to 5% H₂+Ar mixed gas (0.1atm).

2.3.4 Repeatability of sensing and recovery properties

Repeatability of sensing and recovery is another important property of a sensor. Figure 2.9 shows the response for repeated exposure to 5% H$_2$+Ar mixed gas (0.1atm) and air. The quick increase and decreases in current were observed repeatedly, although the current in air tends to increase slightly with the number of cycles.
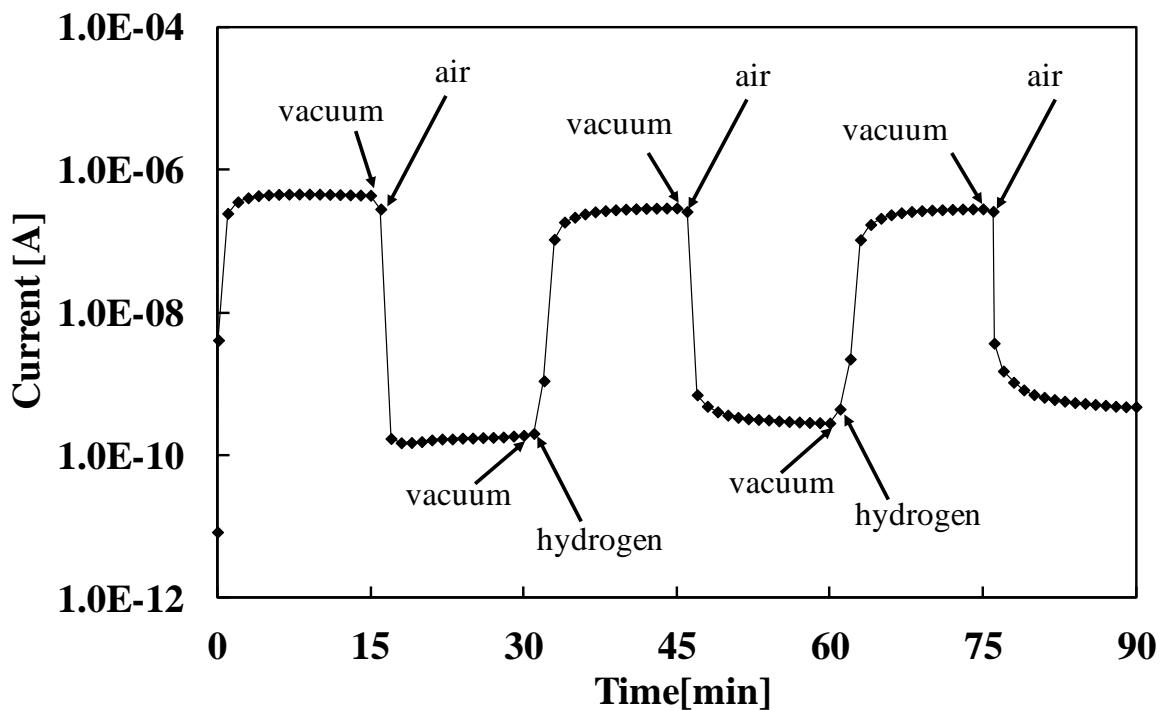
Fig. 2.9 Response to repeated exposure to 5% H$_2$+Ar mixed gas (0.1atm) and air.

There is a few report on SnO$_2$-based gas sensors having sensitivity to hydrogen at room temperature. For example, Shen et al. reported a sensor based on Pd-doped SnO2, for which the resistance changed by a factor of about 10 upon exposure to 1000 ppm hydrogen [3]. As shown above, the sensitivity of the sensors fabricated here (10^4-fold increase for 0.05% H$_2$+Ar mixed gas (0.1 atm)) is superior to those of the sensors previously reported. In addition, the response and recovery speed of our sensors are also relatively fast. This will be owing to large surface/volume ratio of the films and effective Pd doping by the photochemical treatment.

2.4 Conclusion

We fabricated highly sensitive room temperature hydrogen sensors based on SnO$_2$ films. The films were deposited by PCD. A solution containing SnSO$_4$ were dropped onto the glass substrate and irradiated with UV light. After 5 min irradiation, the substrate was washed and the new solution was dropped. The films were fabricated by repeating this process. The sample annealed at 200 °C showed current increase by a factor >10^4 within 1 min for 5% H$_2$+Ar mixed gas (0.1atm) at room temperature. The removal of hydrogen from the ambient caused only a small decrease in the current, but the current decreased by more than three orders of magnitude almost instantly upon subsequent exposure to air.

References

[1] S. Shukla, S. Seal, L. Ludwig, and C. Parish, Sens. Actuators B 97 (2004) 256.

[2] H. T. Wang, B. S. Kang, F. Ren, L. C. Tien, P. W. Sadik, D. P. Norton, J. Peatron, and J. Lin, Appl. Phys. Lett. 86 (2005) 243503.

[3] Y. Shen, T. Yamazaki, Z. Liu, C. Jin, T. Kikuta, and N. Na- katani, Thin Solid Films 516 (2008) 5111.

[4] H. Nakagawa, N. Yamamoto, S. Okazaki, T. Chinzei, and S. Asakura, Sens. Actuators B 93 (2003) 468.

[5] M. Ichimura, K. Shibayama, and K. Masui, Thin Solid Films 466 (2004) 34.

[6] M. Ichimura and T. Sueyoshi, Jpn. J. Appl. Phys. 48 (2009) 015503.

[7] D. Ito and M. Ichimura, Jpn. J. Appl. Phys. 45 (2006) 7094.

[8] G. Korotcenkov, Mater. Sci. Eng. B 139 (2007) 1.

Chapter 3

UV irradiation effects on hydrogen sensors based on SnO$_2$ thin films fabricated by the photochemical deposition

3.1 Introduction

In this chapter, to improve the gas sensor properties further, we attempt to modify the surface condition by 1) changing the annealing ambient from nitrogen to oxygen, and 2) irradiating the sensor surface with the UV light. It has been reported that the light irradiation enhances the sensitivity of the gas sensor [1-3]. In all of such researches, the sensor was irradiated while the sensor response was measured, and the irradiation is thought to promoted the adsorption and desorption of gas molecules, resulting in enhancement of the gas sensors sensitivity. However, for continuous irradiation during the sensing, the power consumption needs to be large and the system cannot be compact. In our study, UV light is once irradiated for one hour before the measurement of the gas sensor. Thus UV light need not be irradiated during the gas sensing; accordingly it is possible to reduce the power consumption and simplify the gas sensor device.

3.2 Experimental detail

As described in chap. 2, the SnO$_2$ films were deposited by 10 times drop-irradiation cycle using the PCD method. And vapor deposition of Au electrodes and Pd doping was performed. In this work, the samples were annealed in nitrogen or oxygen ambient at 200°C. After the sensor fabrication described above, we performed UV irradiation for further improvement of the sensitivity of gas sensors. The UV irradiation by a low-pressure mercury lamp was carried out in air or in vacuum for one hour. The dominant irradiation line is at 254 nm, and the total irradiation power is about 10mW/cm^2. The gas sensor characteristic is evaluated as described in chap. 2. X-ray photoelectron spectrum (XPS) measurement was performed using XPS

PHI-5000 (ULVAC-PHI) with the Al Kα line used as an X-ray source.

3.3 Results

3.3.1 Change in sensitivity with time after the annealing

Figure 3.1 shows the response to 5% H$_2$+Ar mixed gas (0.1atm) introduced into the vacuumed chamber for the same sensors on different date after the sensor fabrication (nitrogen annealing). The sample was kept in the air atmosphere. From those results, it can be seen that the sensor sensitivity was improved with passage of time. Moreover, the response became more rapid, i.e, there is more than one order of magnitude difference in the current at 1 min after the gas introduction between just after the annealing and 4 days later, although the current value before the gas introduction is almost the same. After one week, any further change was not seen, and the response was stabilized. In the following experiments, we used only the fully stabilized samples.
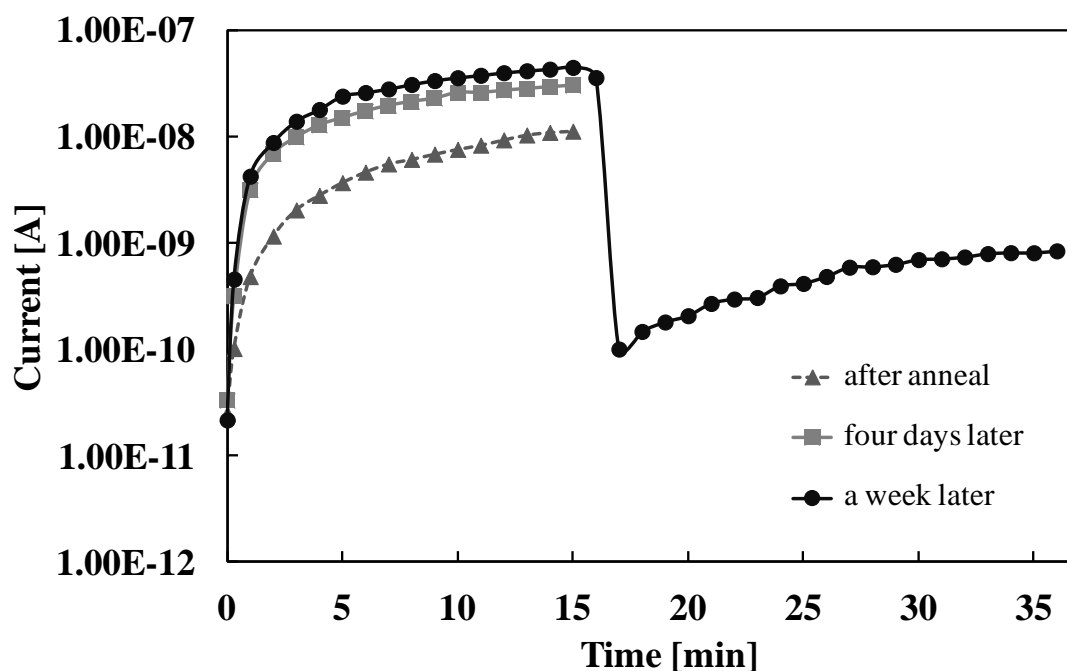

Fig. 3.1 Response to the 5% H$_2$+Ar mixed gas (0.1atm) for the sample measured after different intervals after the annealing. The recovery characteristic is also shown.

These results might be explained considering that amount of oxygen adsorbed on the surface of the thin film increased with time in air, resulting in a more active reaction with hydrogen. Thus we expected that the sensor sensitivity would be improved further when the surface is exposed to oxygen or ozone, and performed the oxygen annealing and UV irradiation treatment, as described in the following sections.

The recovery characteristics are also important characteristics of a gas sensor. The sensor current which is increased with introduction of hydrogen should decrease when hydrogen is removed. As shown in Fig. 3.1, the current first increased upon exposure to 5% H$_2$+Ar mixed gas (0.1atm) and then decreased when the chamber was vacuumed. The observed decrease in current was not large, about 20% within 1 min. When the oxygen gas was introduced up to a pressure of 0.8 atm, the current decreased by more than two order of magnitude almost instantly. As presented in the chap. 2, when air was introduced, the current decreased by more than three order of magnitude almost instantly.

3.3.2 Oxygen-ambient annealing

For the sake of comparison, the annealing temperature was adjusted to 200°C, the same as for the nitrogen annealing. Figure 3.2 shows the response to 5% H$_2$+Ar mixed gas (0.1atm) for the oxygen-annealed sample. The sensor current measured one minute after the gas introduction is larger by about one order of magnitude for the oxygen annealed sample than for the nitrogen annealed sample, although the initial current is almost the same. Figure 3.3 shows the response to low concentration hydrogen (0.05% H$_2$+Ar mixed gas (0.1atm)) for the oxygen annealed sample. The response is slower for the oxygen annealed sample than for the nitrogen annealed sample, although the saturation current is almost the same. After hydrogen was introduced, the current reached the saturation in about 20 minutes for the nitrogen annealed sample, while it takes about 40 min for the current to reach saturation for the oxygen
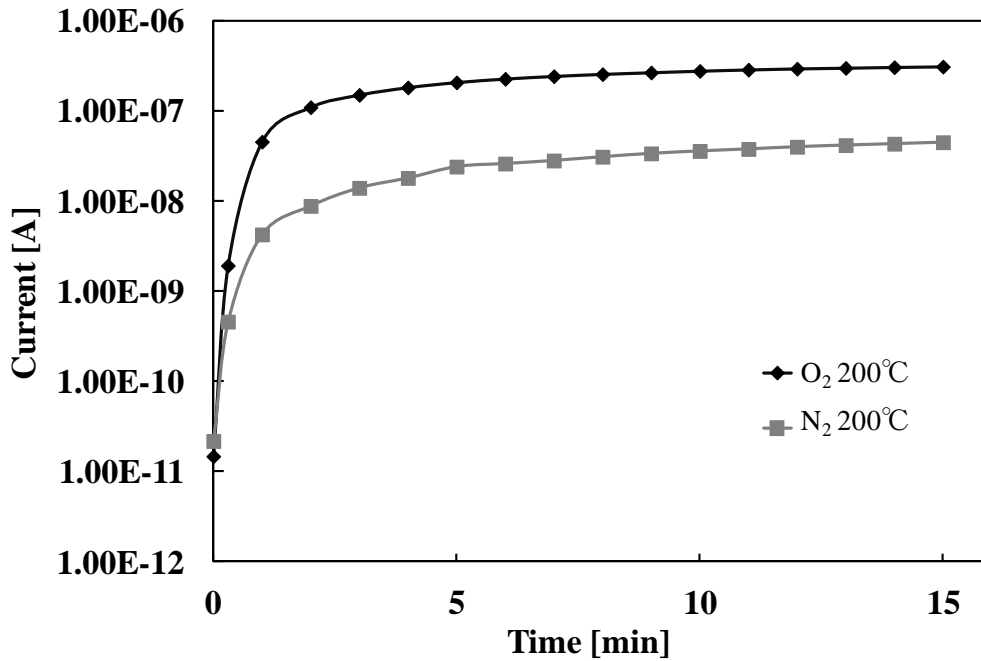
Fig. 3.2 Response to the 5% H$_2$+Ar mixed gas (0.1atm) for the samples annealed in oxygen and nitrogen.
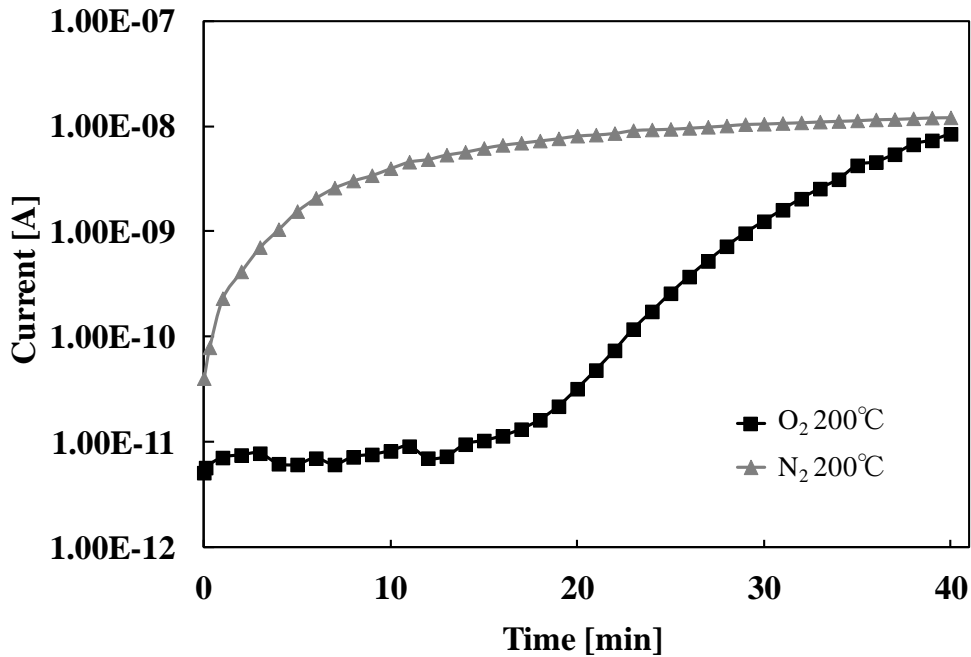
Fig. 3.3 Response to the 0.05% H$_2$+Ar mixed gas (0.1atm) for the samples annealed in the oxygen and nitrogen.

annealed sample. Thus, for the oxygen annealed sample, the sensitivity for the high concentration hydrogen is higher than for the nitrogen annealed one, but the sensitivity for the low concentration hydrogen is inferior.

3.3.3 UV irradiation effects

The samples were put in the air atmosphere or in the vacuum, and irradiated with UV light for one hour using a low-pressure mercury lamp. We used the samples which were annealed in the nitrogen atmosphere at 200°C and fully stabilized by being stored in air for more than one week.

Figure 3.4 shows the response to 5% H_2+Ar mixed gas (0.1atm) before and after the UV irradiation in air. The current increase rate within initial three minutes after introduction of hydrogen is 5.4×10^2 before the UV irradiation, and 4.1×10^3 after the UV irradiation. i.e, the

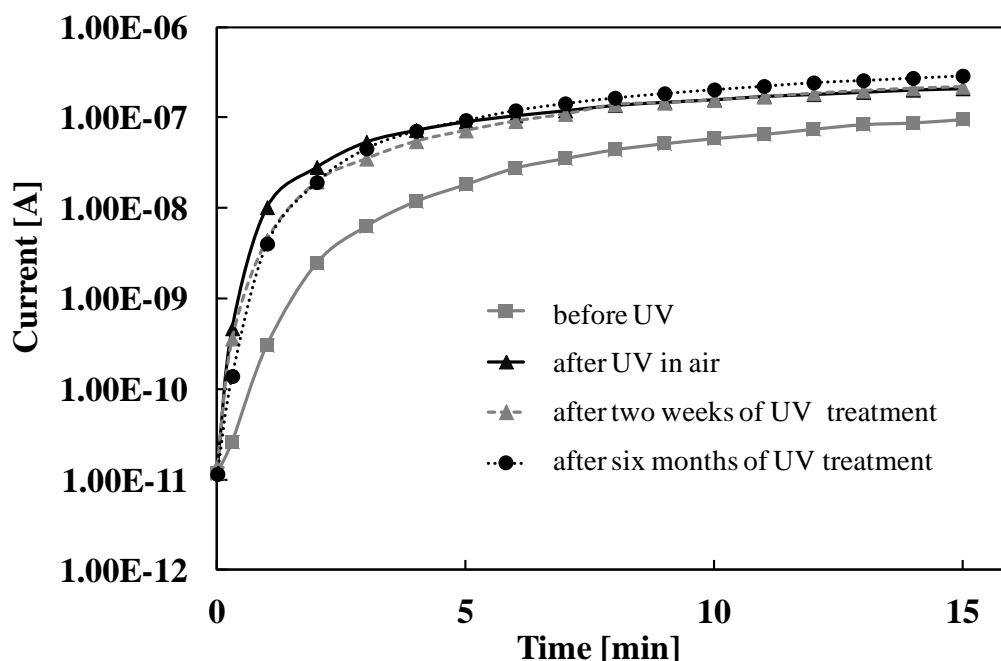**Fig. 3.4 Response to the 5% H_2+Ar mixed gas (0.1atm) for the sample before and after UV irradiation in air.**

current increase rate grew by almost one order of magnitude. This results show that the response was quickened by the UV irradiation in air.

Figure 3.5 shows the response to 5% H$_2$+Ar mixed gas (0.1atm) before and after the UV irradiation in vacuum. The current increase rate within the initial three minutes after introduction of the hydrogen is 6.4×10^2 before the UV irradiation, and 1.3×10^3 after the UV irradiation. To see the effects of the UV irradiation more obviously, the response was measured with 0.05% H$_2$+Ar mixed gas (0.1atm). Figure 3.6 shows the response to 0.05% H$_2$+Ar mixed gas (0.1atm) before and after the UV irradiation in vacuum. As shown in the figure, the current increase rate within the initial ten minutes after introduction of the hydrogen is almost one order of magnitude difference in the reaction sensitivity between before and after UV irradiation in vacuum. Thus, the UV irradiation in vacuum improved the sensitivity of the gas sensor as did the UV irradiation in air.
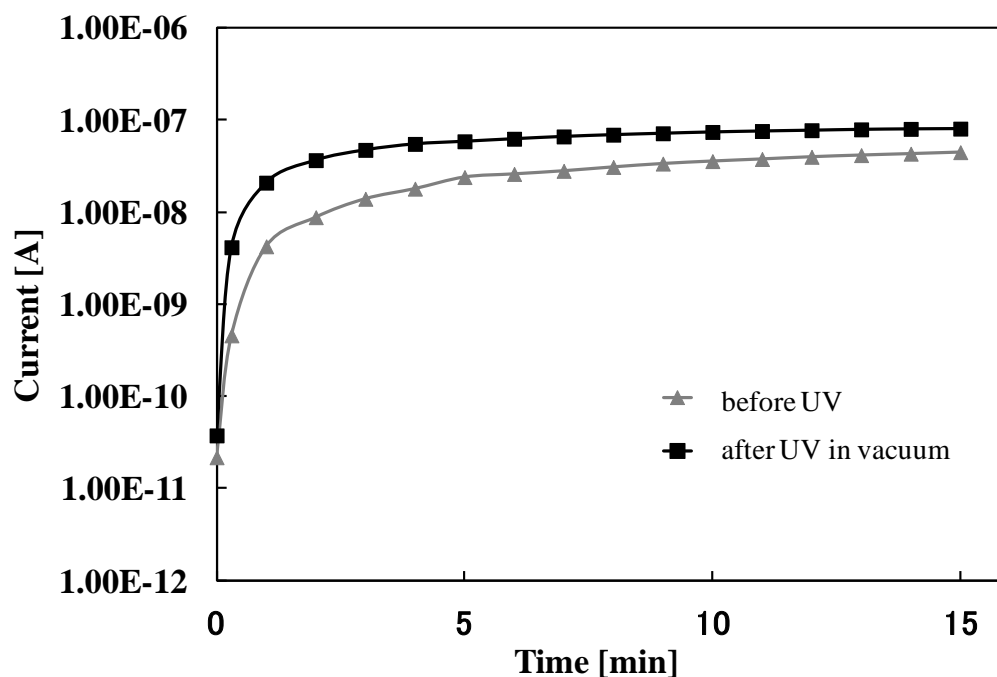

**Fig. 3.5 Response to the 5% H$_2$+Ar mixed gas (0.1atm) for the sample before and
after UV irradiation in vacuum.**
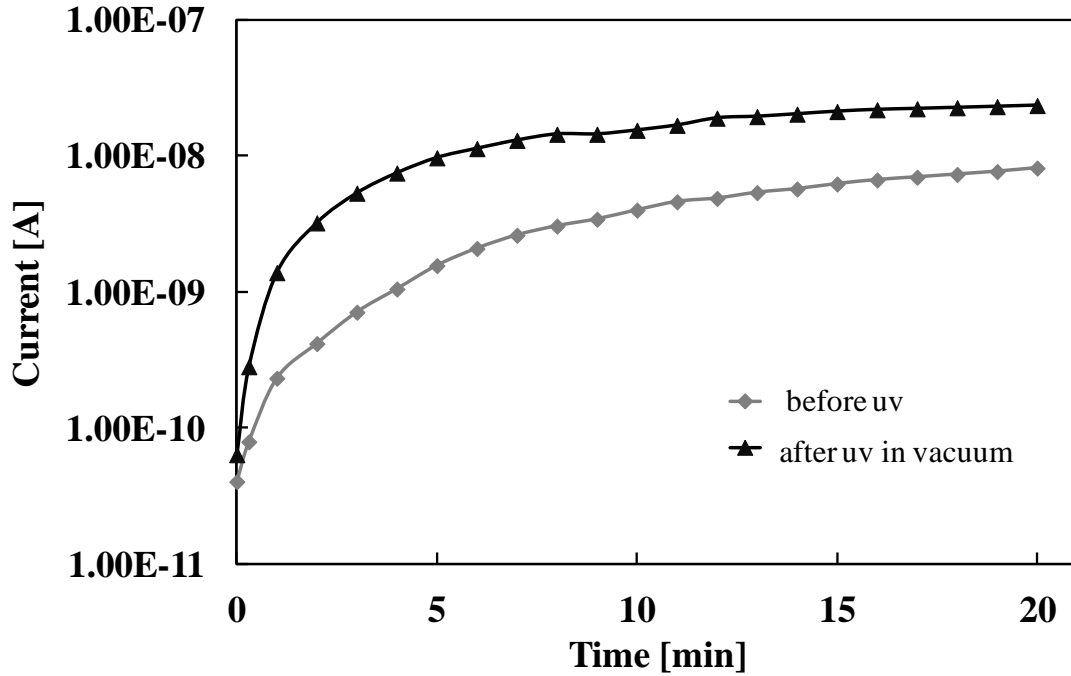
Fig. 3.6 Response to the 0.05% H₂+Ar mixed gas (0.1atm) for the sample before and after UV irradiation in vacuum.

It is necessary to confirm the stability of the sensor after UV irradiation. We examined the sensing property at intervals of two weeks, one month and six months after the UV irradiation. The results are shown in Fig. 3.4. The sensors were kept in the air atmosphere during that intervals. They showed almost the same response after UV irradiation within the experimental uncertainty, and thus we concluded that the response was steady. The stability was also confirmed for the sample UV irradiated in vacuum.

To quantitatively compare the sensing properties, the gas sensitivity, S, is defined as follows:

$S = I_G / I_O$ (1)

where I_G is the current in the testing gas and I_O is the current in the vacuum. The response time was commonly defined as time when the current has reached 90 % of the final value. However, the response of the present sensors can be expressed by a double-exponential function $\exp(-ce^{t/\tau})$ rather than an exponential function $1-e^{-t/\tau}$, where c is a constant and τ the

rate constant of the reaction [4]. Thus the above definition of the response time is not a good measure of the reaction time constant. Here we define the response time t_r as the time when the current I satisfies the following equation:

$\log(I/I_O) = 0.9\log(I_G/I_O)$ (2).

The results for the all treatment are summarized in Table 3.1.

Table 3.1 The sensitivity and response time for the all treatment.

Treatment	N$_2$	O$_2$	UV irradiation (air)		UV irradiation (vacuum)	
			before	after	before	after
S (5% H$_2$)	1.85E+03	1.89E+04	7.37E+03	1.46E+04	1.85E+03	1.93E+03
S (0.05% H$_2$)	2.70E+02	7.16E+03			2.70E+02	3.84E+02
t_r (min) (5% H$_2$)	5	2	7	4	5	2
t_r (min) (0.05% H$_2$)	16	46			16	10

3.3.4 XPS analysis

The sensitivity of our sensors is strongly influenced by the Pd doping. Without Pd doping, the current increased only by a factor of 2-3 with introduction of 5% H$_2$+Ar mixed gas (0.1atm). Therefore, one could suppose that the annealing and the UV irradiation affected the chemical state of Pd. Thus we performed the XPS measurement for the samples annealed in nitrogen, annealed in oxygen, UV irradiated in air and in vacuum, both before and after a surface cleaning by the Ar$^+$ ion sputtering for 6 seconds. The XPS spectra are shown in Figs.

3.7 and 3.8. For all the sample surfaces, the main peak of metal Pd (3d5/2) is located at 335.3 eV. By fitting the observed spectra with Gaussian curves, we obtained relative intensities of the metal Pd peak and the two satellite peaks of Pd located at around 336.3 eV (PdO) and 338.1 eV (PdO$_2$). The results are shown in Fig. 3.9. Before sputtering, the percentage of metal Pd in the oxygen annealed sample was lower than that in the others, which had almost the same percentage of metal Pd. For the sample UV-irradiated in air, the signal of PdO was not observed, and the signal of PdO$_2$ was observed more strongly than the others. After the Ar sputtering, the percentages of metal Pd, PdO and PdO$_2$ were almost the same for the all samples, and Pd was dominantly in the metallic or elemental state.
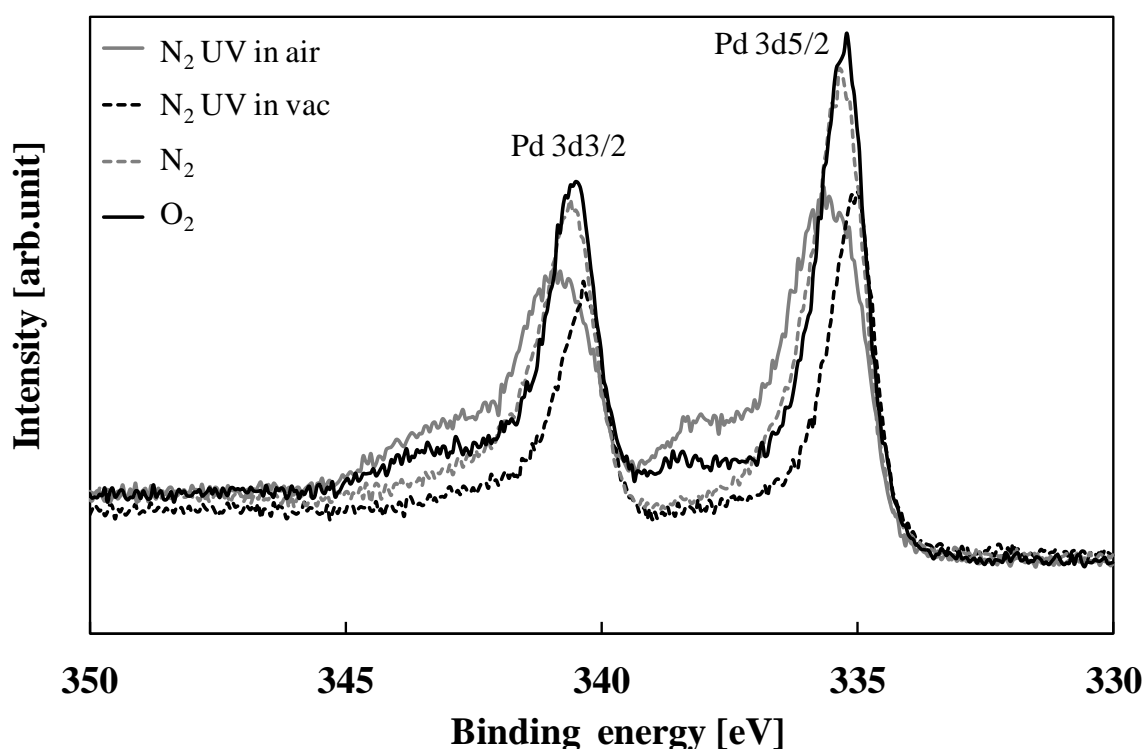

Fig. 3.7 XPS spectra of Pd for the various samples before sputtering.
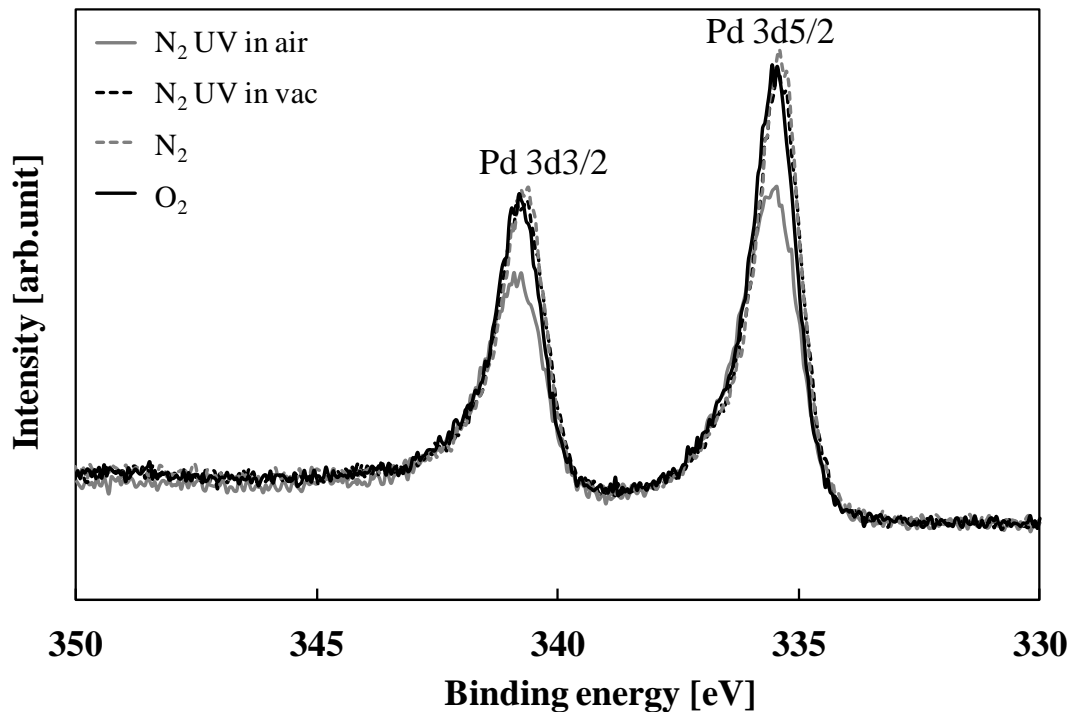
Fig.3.8 XPS spectra of Pd for the various samples after 6 seconds Ar ion sputtering.
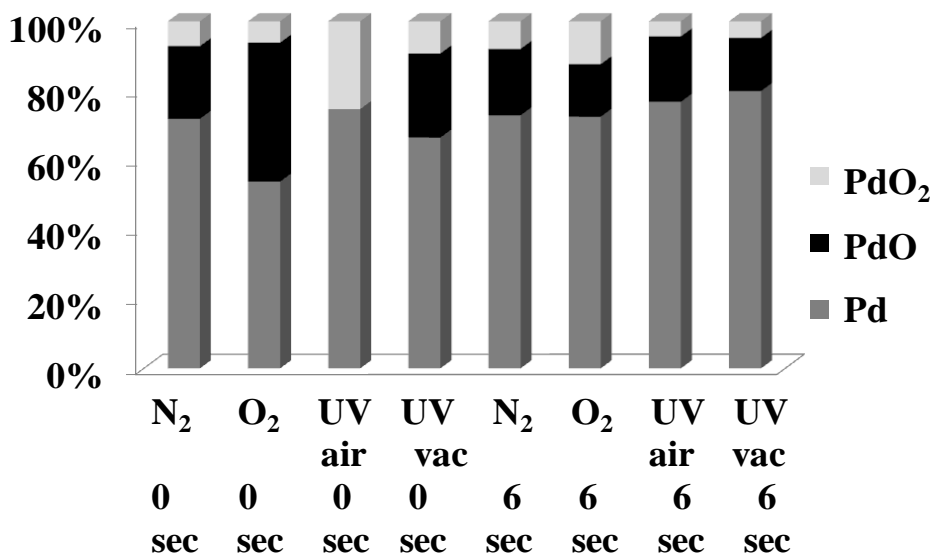

Fig. 3.9 Ratios of Pd species (metal Pd, PdO, and PdO$_2$) in the various samples. "0 sec" means the data taken without Ar sputtering, and "6 sec" after 6 sec Ar sputtering.

3.4 Discussion

For n-type oxide semiconductors, an oxygen atom adsorbed on the surface traps some of the carriers to become a negative ion at the grain boundary. These adsorbed oxygen ions generate a potential barrier between grains, which must disturb the free conduction of the electrons. Under the hydrogen ambient, the oxygen ions are removed by reactions with hydrogen atoms, which leads to decrease in the barrier height and increase in the current. The results given in Fig. 3.1 apparently seem to indicate that the sensitivity is enhanced with increasing amount of pre-adsorbed oxygen. However, the annealing in oxygen did not result in improvement of the sensing properties. Thus the enhancement of sensitivity with time could be due to factors other than amount of adsorbed oxygen.

The UV irradiation in air may enhance the oxygen adsorption, while some oxygen ions may be removed by the irradiation in vacuum [5]. Since both the irradiations in air and in vacuum have similar effects in our experiment, the effects of the UV irradiation cannot be explained by change of the amount of adsorbed oxygen. Then change of the chemical state of surface atoms by UV irradiation may contribute to the improvement of sensitivity. We can consider that the observed high sensitivity of the sensors is mainly due to the metallic Pd. However, we did not find any clear relation between the change in the chemical state of Pd and the change in the sensitivity by the treatments. Considering the above results, the improvement by the UV irradiation is not only due to change in the chemical states of Pd but also other factors.

In general, the H$_2$ gas sensing involves decomposition of H$_2$ molecules at Pd and reaction with oxygen at a reaction site on the SnO$_2$ surface. Thus another possible cause of the improvement observed in this work is the increase in number of reaction sites on the SnO$_2$ surface owing to rearrangement of Sn-O bonding induced by the UV irradiation, although we are unable to obtain evidence. Incorporation of trace amount of impurities could also be the cause of the improvement [2].

3.5 Conclusion

We fabricated highly sensitive room temperature hydrogen sensors based on SnO$_2$ films deposited by the PCD. The sensitivity increased with time after the annealing, and four days after the annealing, the sensor showed current increase by a factor $>10^3$ for 5% H$_2$+Ar mixed gas (0.1atm) at room temperature. We observed significant enhancement in the sensitivity of gas sensors by UV light irradiation by the low-pressure mercury lamp both in air and in vacuum.

References

[1] E. Comini, A. Cristalli, G. Faglia, and G. Sberveglieri, Sens. Actuators B 65 (2000) 260.

[2] Liang Peng, Teng-Feng Xie, Min Yang, and Ping Wang, Sens. Actuators B 131(2008) 660.

[3] Shan-Wei Fan, Arvind K. Srivastava, and Vinayak P. Dravid, Appl. Phys. Lett. 95 (2009) 142106.

[4] M. Ichimura, and T. Sueyoshi, Jpn. J. Appl. Phys . 48 (2009) 015503.

[5] Y. Muraoka, N. Takubo, and Z. Hiroi, J. Appl. Phys. 105 (2009) 103702.

Chapter 4

Deposition and characterization of Sb and Cu doped nanocrystalline SnO$_2$ thin films fabricated by the photochemical method

4.1 Introduction

Doped SnO$_2$ has been fabricated by various techniques, such as sol-gel[1-5], spray pyrolysis[6-8], and sputtering [9]. In chap. 2 and 3, we deposited nanocrystalline SnO$_2$ thin films by a PCD technique and applied them to hydrogen sensors. For the hydrogen sensing, Pd is doped or coated on the SnO$_2$ film surface. The observed sensitivity was extremely high, i.e., the current increased by a factor of about 10^3 for 50 ppm hydrogen at room temperature. However, one drawback of our hydrogen sensor is that the base resistivity is so high that the sensor is not compatible with conventional sensor system.

In this chapter, we attempt to establish the doping technique in PCD of SnO$_2$. Antimony Sb and copper Cu are selected as the impurity to incorporate into SnO$_2$. Sb is commonly used as a donor impurity for SnO$_2$. Cu is known to enhance sensitivity for H$_2$S of a SnO$_2$-based gas sensor[10]. Since PCD is a unique original deposition process, any doping study has not beed reported so far. Once the doping technique is established, it can be utilized for various impurity elements to modify electrical and optical propertis and also to control sensing characteristics of the SnO$_2$ films.

4.2 Experimental detail

Doped and undoped SnO$_2$ thin films were fabricated by the drop-PCD method. The undoped SnO$_2$ films were deposited as described in chap.2. We obtained a SnO$_2$ film with a thickness of about 0.15 μm by repeating the drop-irradiation cycle 10 times. For impurity doping, a solution for the SnO$_2$ deposition and another solution for the doping were prepared

separately. A small amount of each of these solutions was alternately dropped on the glass substrate, and irradiated by the UV light. In this process, a thin SnO$_2$ film is deposited in the first drop-irradiation cycle, and then in the next cycle, impurity atoms will replace some of the Sn atoms in the deposited films. The Sb doping solution is a 2-propanol solution containing 2 mmol/L of SbCl$_3$. For the Cu doping, the following two aqueous solutions were prepared. One is a solution including 2 or 20 mmol/L CuSO$_4$ (1). The other one is a solution containing 20 mmol/L CuSO$_4$ and 50 mmol/L Na$_2$SO$_3$ (2) with solution pH about 7.2 (unadjusted). We repeated the drop-irradiation cycles 20 times (10 times for the SnO$_2$ deposition and 10 times for the doping, alternately) and obtained doped SnO$_2$ thin films with a thickness of around 0.10~0.20 μm. We confirmed that for both Sb and Cu, no film was deposited when only the doping solution was dropped and irradiated. The SnO$_2$ thin films were annealed in nitrogen ambient at 200°C, 300°C and 400°C.

The compositional analysis was carried out by Auger electron spectroscopy (AES) using the model JEOL JAMP 7800 Auger microprobe at probe voltage 10 kV and current 2×10^{-8} A. An argon-ion sputtering with acceleration voltage 3 kV and current 20 mA was used to sputter the film surface. The optical transmission measurement was performed using the JASCO U-570 spectrometer with the glass substrate as the reference. X-ray diffraction (XRD) was measured using Rigaku Smartlab diffractometer with Cu K radiation source. The surface morphology of the film was analyzed by scanning electron microscope (SEM; Hitachi S-3000H), keeping the acceleration voltage at 25 kV and magnification at 6000. In addition, indium electrodes (electrode size 1x1 mm^2) were thermally evaporated and the current-voltage (I-V) characteristics were measured for the as-deposited as well as the annealed films. The conduction type was judged by the hot-probe method. The van der Pauw–Hall measurement was performed at room temperature for the 400°C annealed films using TOYO Corporation Model ResiTest 8310.

4.3 Results and discussion

4.3.1 Compositional properties

Figure 4.1 shows the AES spectra of the as-deposited SnO$_2$ thin films doped with Sb and Cu after 10 s Ar-ion sputtering. The solution containing 2 mmol/L CuSO$_4$ was used for the Cu doping. From those spectra, contents of impurity elements were evaluated using standard Auger efficiencies for elements. (The actual Auger intensity is known to depend on the matrix material and thus the following composition analysis could be regarded as an order-of-magnitude estimate.) The Sb/Sn atomic ratio in the film is as high as 0.53. In contrast, Cu content is relatively low, i.e., the Cu/Sn atomic ratio is about 0.08, when the solution containing 2 mmol/L CuSO$_4$ was used. The Cu content did not change significantly even when the CuSO$_4$ concentration in the doping solution was increased to 20 mmol/L. To enhance Cu content, solution (2) was used, i.e, 50 mmol/L Na$_2$SO$_3$ was added to the solution
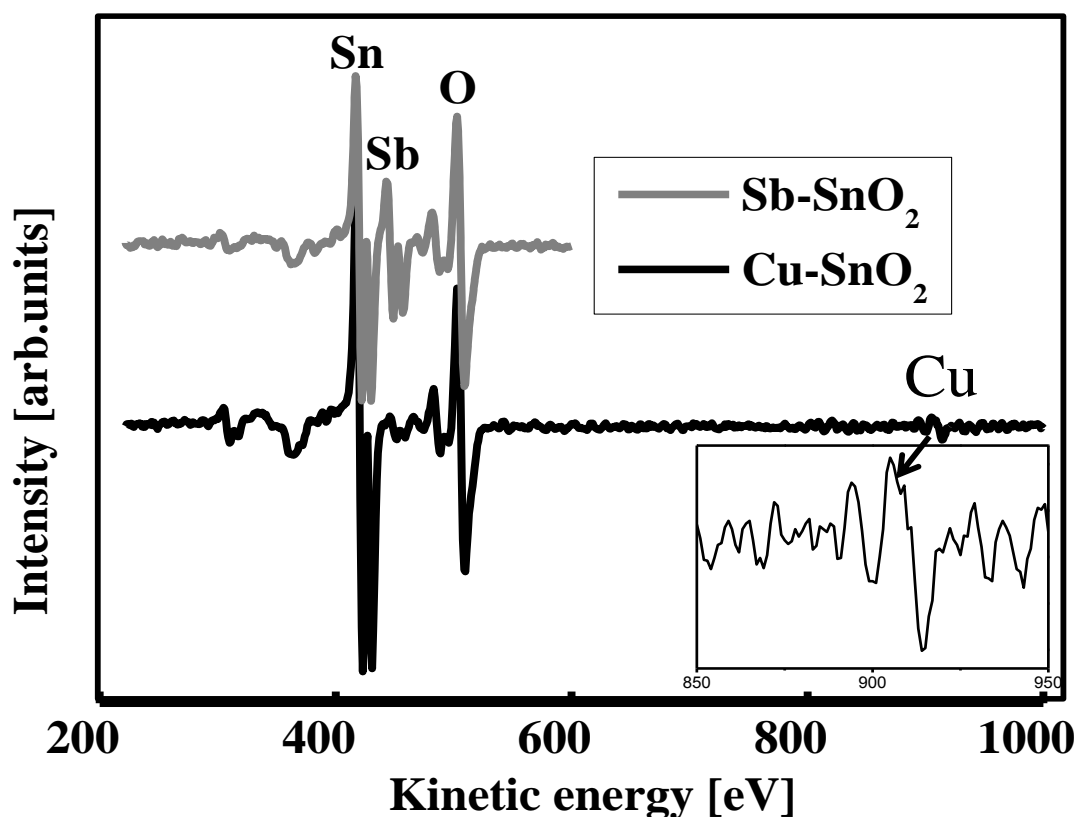

Fig. 4.1 AES spectra of the doped SnO$_2$ thin films. Inset shows the expanded Cu-doped SnO$_2$ AES spectrum near the position of Cu peak.

containing 20 mmol/L of CuSO$_4$. It was reported that the formation of the copper oxide is promoted by using the SO$_3{}^{2-}$ ions as a reducing agent [11]. Thus, if the SO$_3{}^{2-}$ ions act as a reducing agent in the PCD process, incorporation of Cu atoms into the film could also be promoted. However, the Cu/Sn atomic ratio was about 0.10, i.e., did not significantly increase compared with the case of solution (1).

The Cu content in the Cu-doped films did not increase significantly even when the CuSO$_4$ content of the doping solution was increased. This result may be explained as follows. In the photochemical doping process of Cu, Cu atoms would replace the Sn atoms in the vicinity of the SnO$_2$ film surface during the photo-irradiation. Such photochemical doping of Pd into a SnO$_2$ film has been observed in our previous works. In this process, only a limited number of Sn atoms in the vicinity of the surface may be available for the replacement, and thus once all of them are replaced by the impurity atoms, the replacement could not proceed further. Therefore, the Cu content in the film did not increase with increasing amount of CuSO$_4$ concentration in the solution. On the other hand, Sb content is considerably larger. This indicates that Sb atoms replaced not only the surface atoms but also Sn atoms in the bulk. Then, we can consider a possibility that an Sb-rich phase was formed in the film.

4.3.2 Optical properties

From the optical transmission spectra shown in Fig. 4.2, it can be seen that the doped and undoped SnO$_2$ thin films have fairly high transmission in the visible region of the spectrum. The optical transmissions of all the samples except for Sb-doped SnO$_2$ are more than 80% in the visible region, whereas the transmission of the Sb-doped SnO$_2$ film is slightly lower than those of others. The optical band gap energy was calculated from the classical relation for direct-band optical adsorption.
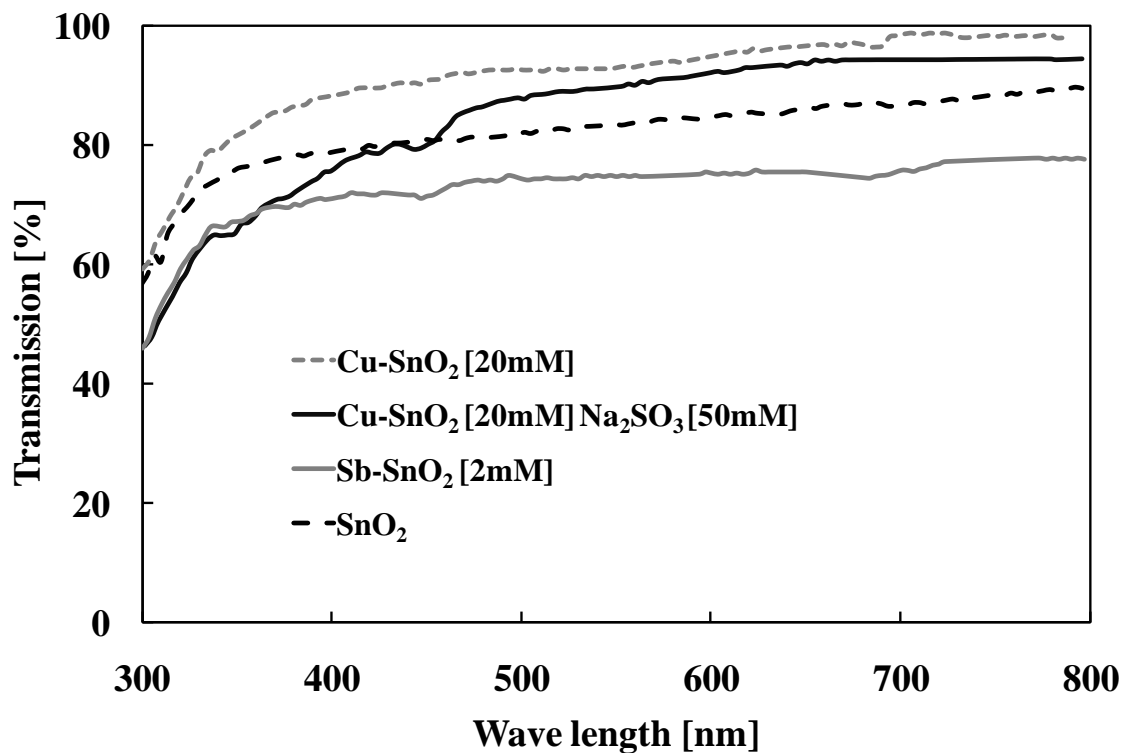
Fig. 4.2 Optical transmission of the undoped and doped SnO$_2$ thin films.
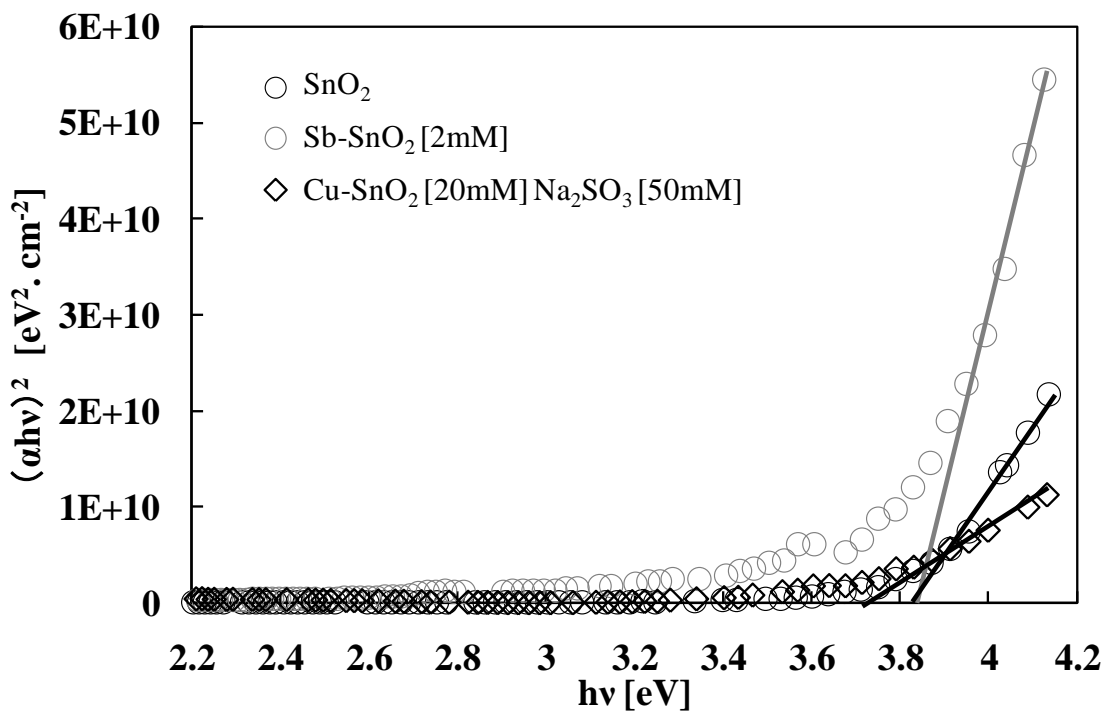

Fig. 4.3 Plot of $(\alpha h\nu)^2$ against $h\nu$ of the undoped and doped as-deposited films.

$$\alpha = k(h\nu - E_g)^{1/2}/h\nu \qquad (1)$$

where α is the absorption coefficient, k a constant, E_g the band gap and $h\nu$ the photon energy. Figure 4.3 shows the variation of $(\alpha h\nu)^2$ versus $h\nu$, which is linear in the higher energy domain, indicating a direct optical transition. The band gap energy E_g was obtained by extrapolating the linear portion of the graph to the energy axis at $\alpha = 0$. The obtained band gap values are around 3.7~3.8 eV for both the undoped and doped SnO$_2$ thin films.

4.3.3 Surface morphology

Figures 4.4 (a-d) shows the morphology of the as-deposited films. There is no apparent difference in morphology between the undoped film (Fig.(a)) and the Sb-doped film (Fig.(b)). The morphology of the Cu-doped SnO$_2$ thin films is shown in Figs. 4.4 (c) and (d). Grain
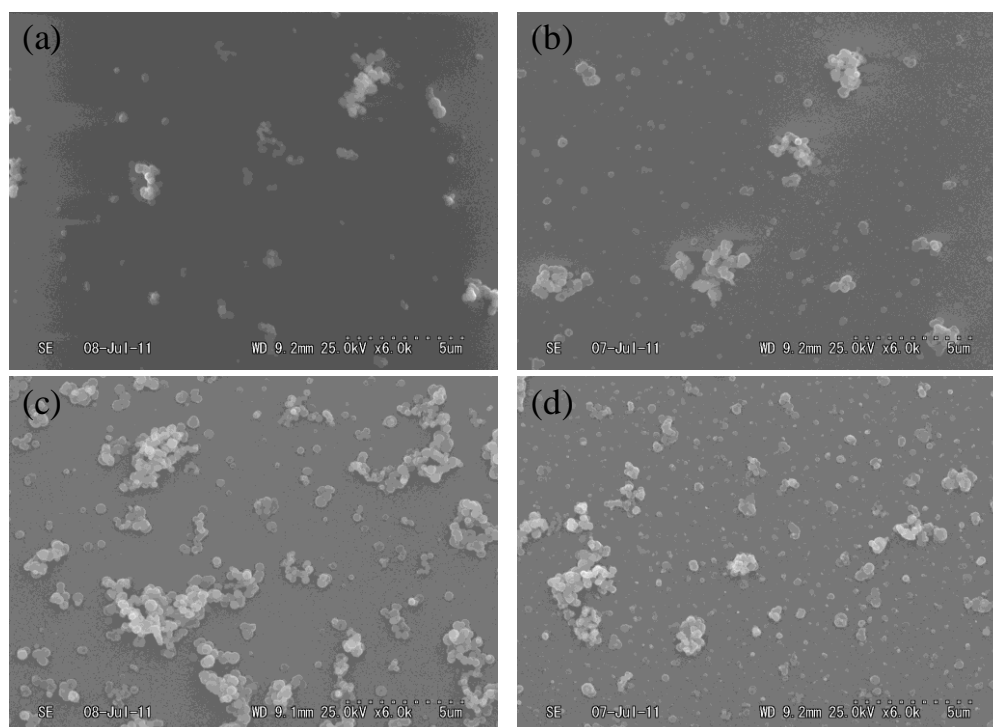

Fig. 4.4 SEM images of the various as-deposited SnO$_2$ films:

(a) undoped SnO$_2$; (b) Sb-SnO$_2$;

(c) Cu-SnO$_2$ [2mM CuSO$_4$]; (d) Cu-SnO$_2$ [20mM CuSO$_4$ and 50mM Na$_2$SO$_3$].

structure can be seen more clearly for the Cu-doped films than for the undoped film. The SEM images of the 400°C annealed films shown in Figs. 4.5 revealed that no significant difference on the surface morphology due to the annealing.
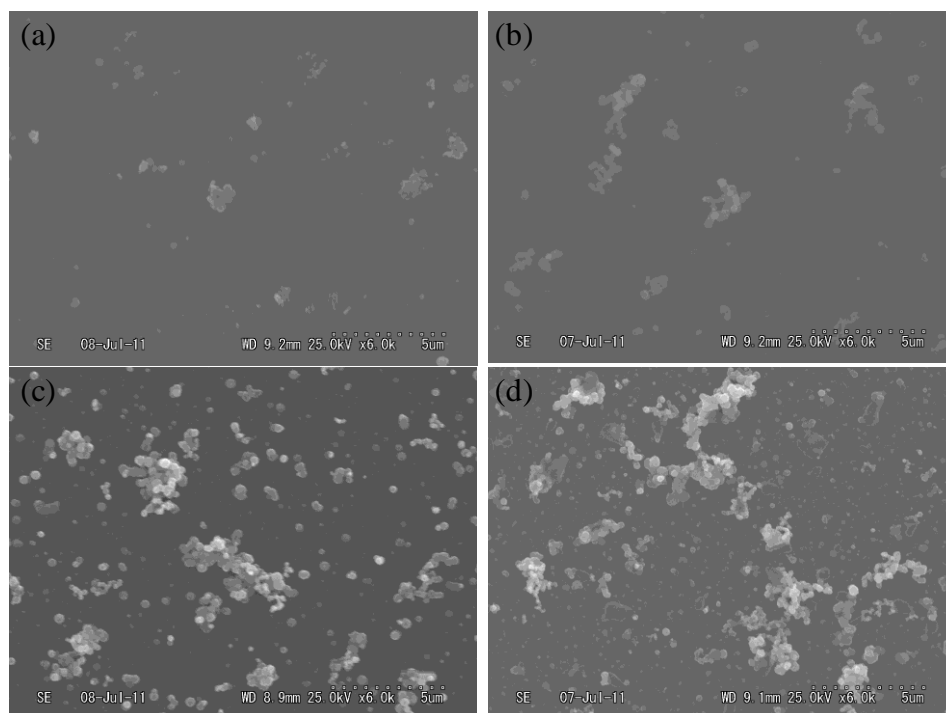
Fig. 4.5 SEM images of the various 400°C annealed SnO$_2$ films:

(a) undoped SnO$_2$; (b) Sb-SnO$_2$;

(c) Cu-SnO$_2$ [2mM CuSO$_4$]; (d) Cu-SnO$_2$ [20mM CuSO$_4$ and 50mM Na$_2$SO$_3$].

4.3.4 Electrical and structural properties

Figure 4.6 shows the plots of resistivity for the undoped and doped samples annealed at different temperatures (the data for the as-deposited film were plotted at 27°C). The measured resistivity of the films deposited under the same condition shows scatter of about ± 10 %, which will be due to nonuniformity of the film. The resistivity higher than 10^6 Ωcm cannot be measured by our measurement system. Therefore, the electrical resistivity could be higher than 10^6 Ωcm for the as-deposited films and the films annealed at 200 and 300 °C. The

resistivity was decreased by the 400 °C annealing. The conduction type judged by the hot
probe method was n-type for all the samples annealed at 400°C.
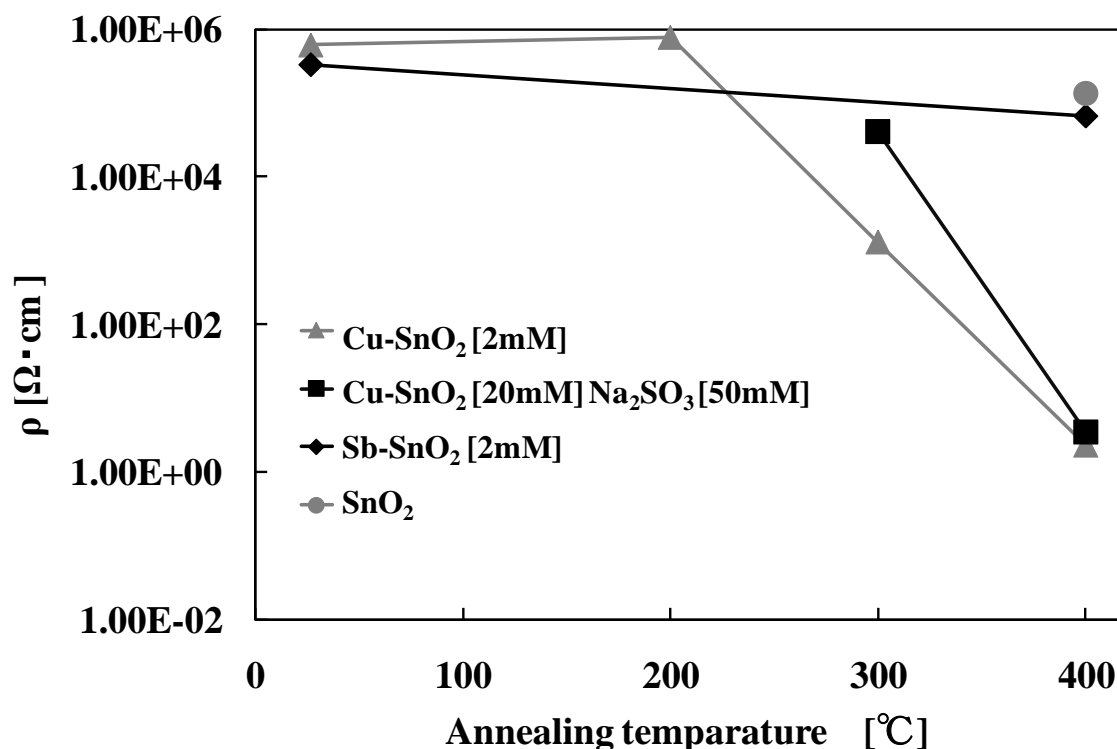
Fig. 4.6 Resistivity of the various SnO$_2$ samples annealed at different temperatures.

Sb is a group V element and thus can act as a donor if it substitutes Sn, which is a group IV
element. However, in our experiment, the Sb doping did not result in decrease in resistivity.
We can consider two reasons for this. The first one is the change in the film morphology. If
the film becomes more porous, the observed resistivity will not be decreased. The
morphology of the Sb-doped film is shown in Fig. 4.4(b). It was found that there is no
apparent change in the morphology compared with the undoped film (Fig. 4.4 (a)). Thus the
morphology could not be the dominant factor. However, since there is no apparent change in
the morphology compared with the undoped film, the morphology could not be the dominant
factor. The second possible reason is that the Sb atoms did not replace Sn atoms but formed a
separate high resistivity phase, probably Sb$_2$O$_3$. As discussed above, the AES results are
considered to indicate the formation of Sb-rich oxide. For doping of Sb into the substitutional

sites, formation of the separate phase needs to be suppressed by, for example, using a much more diluted SbCl$_3$ solution.

The resistivity of the film was found to become significantly lower by the Cu doping, as shown in Fig. 4.6. Any further decrease in the resistivity of the Cu-doped SnO$_2$ was not seen when the concentration of Cu in the doping solution was increased from 2 mmol/L to 20 mmol/L. This is consistent with the AES results that the Cu content was not increased by increasing CuSO$_4$ concentration in the solution. The carrier concentration and mobility were determined by the Hall measurements at room temperature for the film annealed at 400°C. For the Cu-doped SnO$_2$ films (2mM CuSO$_4$), the results showed that the electron concentration is 3×10^{16} cm^{-3} and the carrier mobility 0.4 cm^2 V^{-1} s^{-1}. Since there is scatter of about ± 10 % in the resistivity value, the same amount of scatter is expected for the Hall measurement results. The measurement failed for the undoped film because of its high resistivity.

In contrast to Sb, substitutional Cu atoms in SnO$_2$ are not regarded as a donor since Cu has a smaller number of valence electrons than Sn. Copper oxide is conductive but usually shows p-type conductivity, and thus the observed decrease in resistivity will not be due to the formation of the copper oxide phase. One possible explanation of the reduced resistivity of the Cu-doped films is that the grain became larger due to the Cu doping. The growth of grain size will diminish effects of grain boundaries and reduce the resistivity. A few groups have reported deposition of Cu-doped SnO$_2$ films so far. In ref.[8], it was reported that Cu doping leads to increase in grain size in spray pyrolysis deposited SnO$_2$ films, while in ref.[7], it was reported that Cu doping has minor effects on morphology and microstructure of the films obtained by electrostatic spray deposition. Electrical resistivity was not given in those previous papers. Our SEM results show that there are a larger number of grains for the Cu-doped films, but since the grains are separated from each other, they may not contribute to the electrical conduction. On the other hand, for all the samples annealed at 400°C, XRD patterns were recorded. As shown in Fig. 4.7, we did not observe any clear peaks which can

be attributed to the deposit. This indicates that the films are amorphous or nanocrystalline irrespective of doping and that increase in the grain size is not significant even after the annealing. Thus the grain growth is not considered to be the main reason for the reduced resistivity of the Cu-doped films.
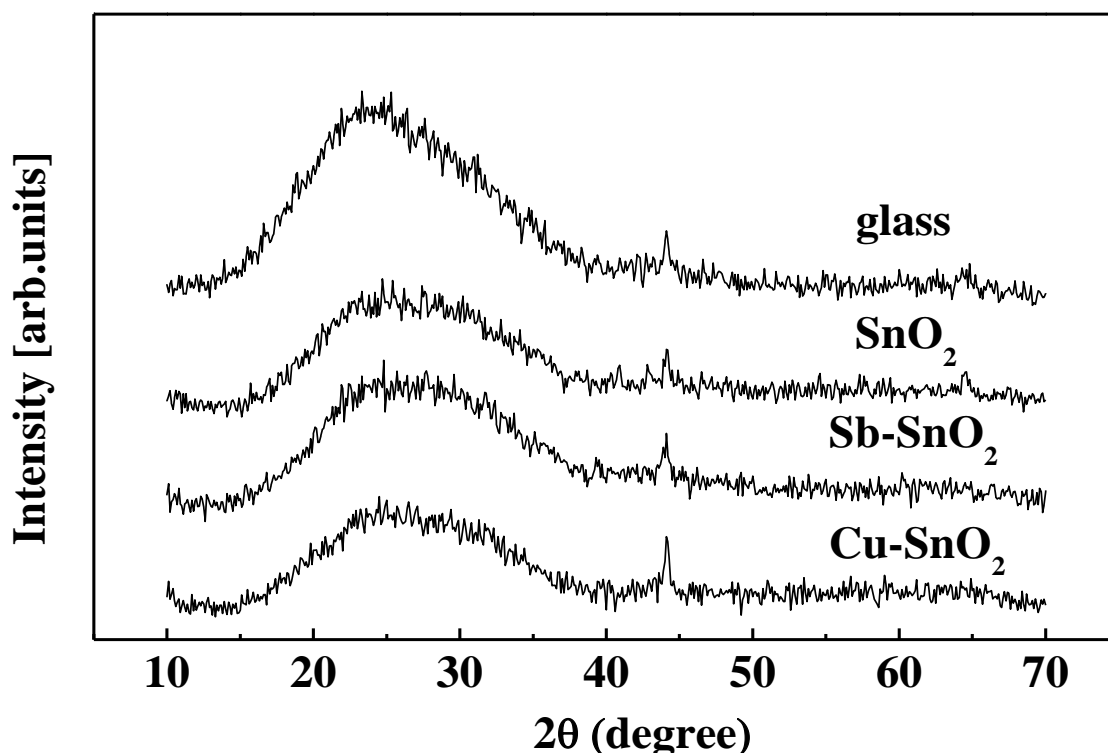
Fig.4.7 X-ray diffraction patterns of various 400°C annealed SnO₂ films.

Another possible explanation for the resistivity reduction is that some portion of the doped Cu atoms are at interstitial sites. Cu^+ or Cu^{2+} ions at interstitial sites will act as a donor and increase electron concentration. For the Cu-doped SnO₂ films annealed at 400°C, the Hall measurement results showed that the electron concentration is $3 \times 10^{16} \, cm^{-3}$, and the carrier mobility 0.4 cm^2 V^{-1} s^{-1}. The mean free path estimated from the mobility is small, of the order of 0.01 nm, which is consistent with the fact that the grain growth is not significant according to the XRD results. Therefore, the enhanced conductivity will be mainly due to enhanced electron concentration, and thus the doped Cu atoms are thought to act as a donor. However,

the Cu/Sn ratio determined from AES is about 0.1, which corresponds to a concentration much higher than the electron concentration. Thus the majority of the doped Cu atoms would be at substitutional sites, and only a small percentage of the Cu atoms are activated as a donor.

4.4 Conclusion

Sb-doped and Cu-doped SnO$_2$ thin films have been deposited on glass substrates using the PCD technique. The optical transmission of the film is fairly high in the visible region, and the band gap obtained is 3.7 - 3.8 eV. The resistivity of the 400°C annealed films is significantly lower for the Cu-doped film than for the undoped and Sb-doped films. The Hall measurement results show that the electron concentration is 3×10^{16} cm^{-3} for the Cu-doped SnO$_2$ films annealed at 400°C.

References

[1] J.P. Chatelon, C. Terrier, E. Bernstein, R. Berjoan, and J.A. Roger, Thin Solid Films 247 (1994) 162.

[2] X. P. Cao, L. L. Cao, W. Q. Yao, and X.Y. Ye, Thin Solid Films 317 (1998) 443.

[3] Z. G. Ji, Z. J He, Y. L Song, K. Liu, and Z. Z. Ye, J. Cryst. Growth 259 (2003) 282.

[4] Y. Hu, and S. -H. Hou, Mat. Chem. Phys. 86 (2004) 21.

[5] T. N. Soitah, C. H. Yang, and L. Sun, Mat. Sci. Semicond. Proc. 13 (2010) 125.

[6] S. Shanthi, C. Subramanian, and P. Ramasamy, J. Cryst. Growth 197 (1999) 858.

[7] C. M. Ghimbeu, R.C. V. Landschoot, J. Schoonman, and M. Lumbreras, J. European Ceramic Soc. 27 (2007) 207.

[8] G. Korotcenkova, and S. D. Hana, Mat. Chem. Phys. 113 (2009) 756.

[9] T. Y. Yang, X.B. Qin, and H. H. Wang, Thin Solid Films 518 (2010) 5542.

[10] J. Tamaki, T. Maekawa, N. Miura, and N. Yamazoe, Sens. Actuators B 9 (1992) 197.

[11] M. Muhibbullah, and M. Ichimura, Jpn. J. Appl. Phys. 49 (2010) 081102.

<div align="right">

Chapter 5

Deposition of Fe doped nanocrystalline SnO₂ thin films by the photochemical deposition method

</div>

5.1 Introduction

Tin dioxide SnO_2 is a technologically important material due to its various applications such as gas sensors, chemical sensors, and transparent conducting thin films. For most of those application, doping of impurities is needed to modify its conductivity, optical absorption and gas sensitivity. In most cases, electrical conductivity has been controlled by doping antimony or fluorine [1-5]. Recently, Fe-doped SnO_2 has attracted a lot of interest because Fe doping can modify conductivity, gas sensitivity, and band gap. In the past, Fe-doped SnO_2 thin films have been obtained by sol-gel [6,7] and spray pyrolysis[8,9]. So far, there is no report on Fe-doped SnO_2 thin films by the PCD technique. In the previous chapter, we reported deposition of SnO_2 thin films doped with Sb and Cu by the PCD technique. We obtained lower resistivity for the Cu-doped film than for the undoped and Sb-doped films. In this chapter, iron Fe is selected as the impurity to incorporate into SnO_2. Electrical and optical properties of Fe-doped SnO_2 are investigated and compared with the previous chapter results.

5.2 Experimental detail

Fe doped SnO_2 thin films were fabricated by the drop-PCD method. The Fe doping was attempted by two kinds of methods. In the first one, 2 mmol/L $FeSO_4$ was mixed in SnO_2-deposition solution as described in chap. 2, and the films were deposited by repeating the drop-irradiation cycle 10 times. In the second one, a solution for the SnO_2 deposition and another solution for the doping were prepared separately. A small amount of each of these solutions was alternately dropped on the glass substrate, and irradiated by the UV light. In this process, a thin SnO_2 film is deposited in the first drop-irradiation cycle, and then in the next

cycle, impurity atoms will replace some of the Sn atoms in the deposited films. The doping solution containing 20 or 200 mmol/L FeSO$_4$ with 20 mmol/L Na$_2$SO$_3$. It was reported that the formation of metal oxide is promoted by using the SO$_3^{2-}$ ions as a reducing agent [10]. Thus, if the SO$_3^{2-}$ ions act as a reducing agent in the PCD process, incorporation of Fe atoms into the film could also be promoted. We repeated the drop-irradiation cycles 20 times (10 times for the SnO$_2$ deposition and 10 times for the doping, alternately) and obtained doped SnO$_2$ thin films with a thickness of around 0.15 μm. We confirmed that no film was deposited when only the doping solution was dropped and irradiated. The SnO$_2$ thin films were annealed in nitrogen ambient at 200°C, 300°C and 400°C.

The Auger electron spectroscopy (AES) analysis and scanning electron microscopy (SEM) observation were carried out using the model JEOL JAMP- 9500F at probe voltage 10 kV. An argon-ion sputtering with acceleration voltage 2 kV and current 2.6 μA was used to sputter the film surface. The optical transmission measurement was performed using the JASCO U-570 spectrometer with the glass substrate as the reference. In addition, indium electrodes (electrode size 1x1 mm^2) were thermally evaporated and the current-voltage characteristics were measured for the as-deposited as well as the annealed films. The conduction type was judged by the hot-probe method.

5.3 Results and Discussion

5.3.1 Compositional properties

In the AES measurement, the peak of Fe was not observed when the FeSO$_4$-mixed solution was used. Thus the Fe content is less than the detection limit of AES (a few percents). On the other hand, the Fe signal was observed for the films deposited using the separate doping solution. Figure 5.1 shows the AES spectra of the as-deposited SnO$_2$ thin films doped with Fe after 10 s Ar-ion sputtering. From those spectra, contents of impurity elements were evaluated using standard Auger efficiencies for elements. The Fe/Sn atomic ratios were about 0.07 and

0.11 with the doping solution containing 20 or 200 mmol/L FeSO$_4$ respectively. It should be noted that although Na ions are contained in the deposition solution, no Na signal was detected in the AES spectra. This will be because Na has a high ionization tendency and thus remains in the solution as an ion.
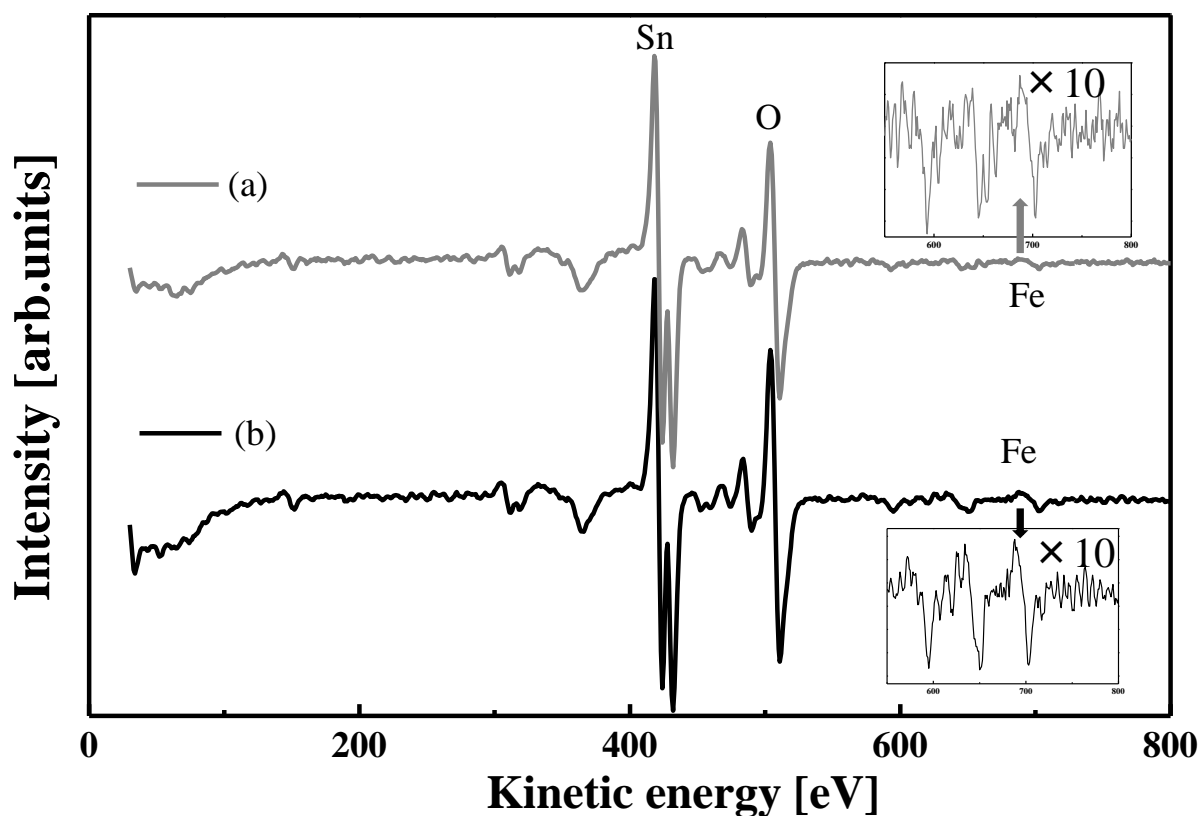

Fig. 5.1 AES spectra of the Fe-doped SnO$_2$ films deposited using the separate doping solution containing (a) 20mmol/L FeSO$_4$, and (b) 200mmol/L FeSO$_4$. The inset shows the expanded AES spectra near the position of Fe peak.

5.3.2 Optical properties

Figure 5.2 shows the optical transmission of the undoped SnO$_2$ film and the Fe-doped film deposited by the separate doping solution containing 20mmol/L. The result shows that both the Fe-doped and undoped SnO$_2$ thin films have fairly high transmission in the visible region of the spectrum. The optical transmissions result is the almost same for the Fe-doped SnO$_2$

films deposited using the FeSO$_4$-mixed solution and the separate doping solution containing 200mmol/L FeSO$_4$. The optical band gap energy was calculated from the classical relation for direct-band optical adsorption.

$$\alpha = k(h\nu - E_g)^{1/2}/h\nu \qquad (1)$$

where α is the absorption coefficient, k a constant, E_g the band gap and $h\nu$ the photon energy. Figure 5.3 shows the variation of $(\alpha h\nu)^2$ versus $h\nu$, which is linear in the higher energy domain, indicating a direct optical transition. The band gap energy E_g was obtained by extrapolating the linear portion of the graph to the energy axis at $\alpha = 0$. The obtained band gap values are around 3.8~3.9 eV for both the undoped and Fe-doped SnO$_2$ thin films.
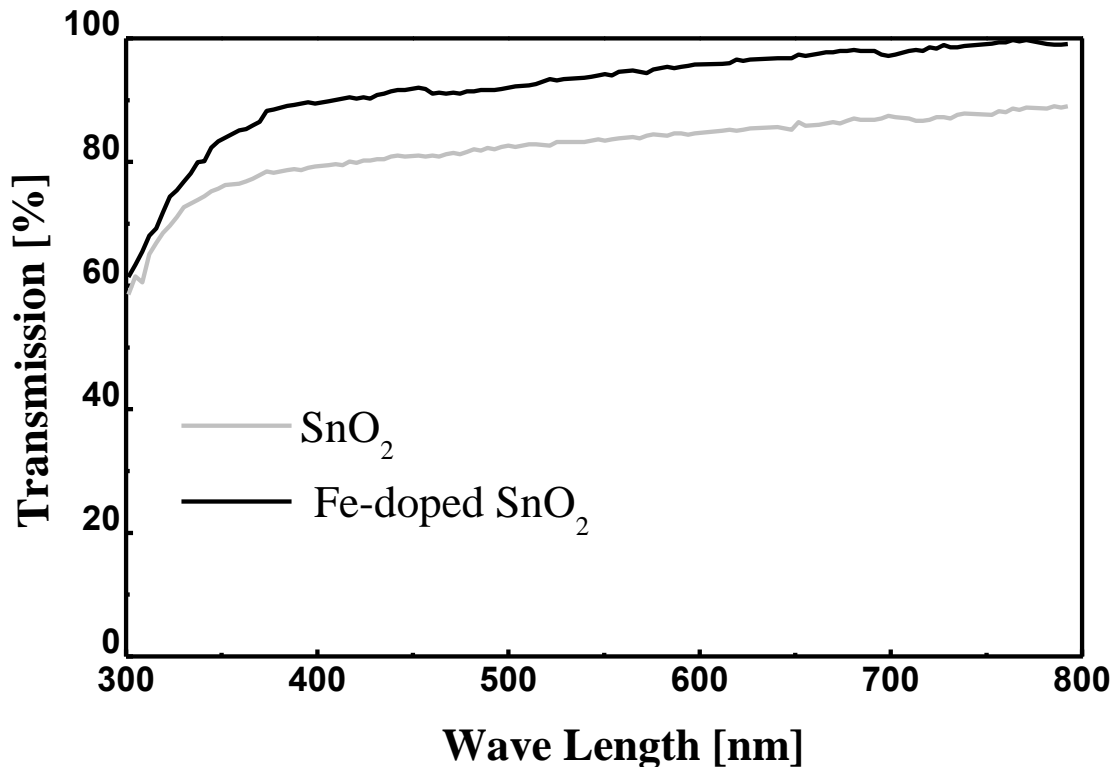

Fig. 5.2 Optical transmission of the undoped and Fe-doped as-deposited films. The Fe doped film was deposited using the separate doping solution containing 20mmol/L FeSO$_4$.
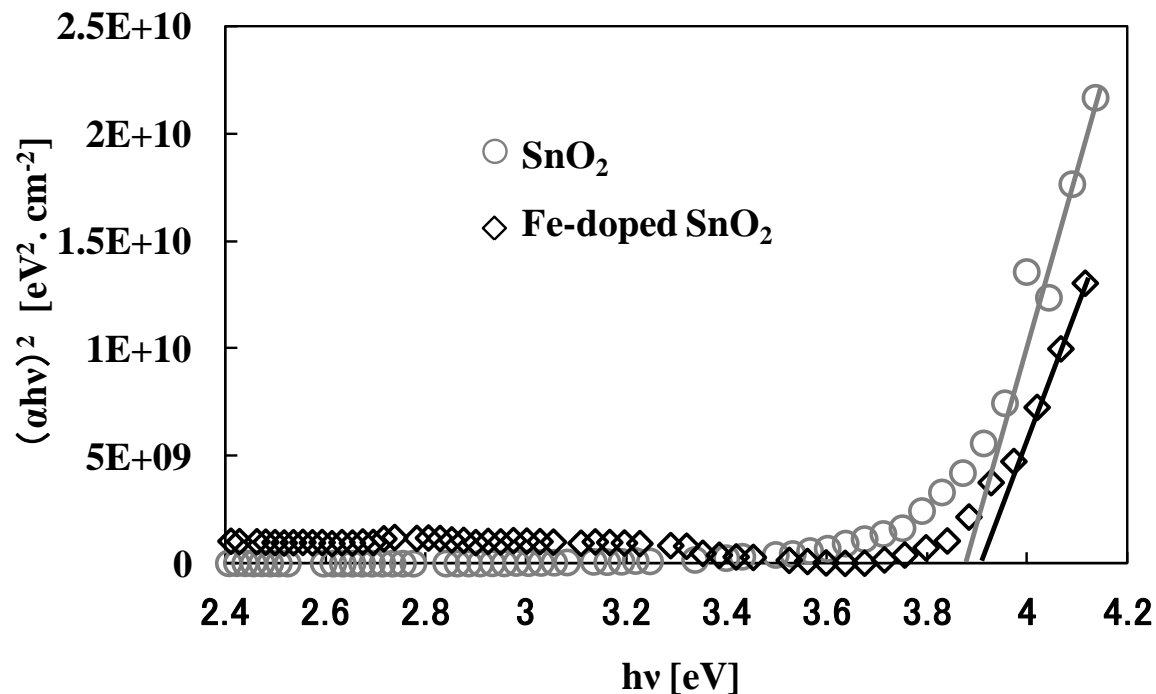
Fig. 5.3 Plot of $(\alpha h\nu)^2$ against $h\nu$ of the undoped and Fe-doped SnO$_2$ as-deposited films. The Fe doped film was deposited using the separate doping solution containing 20mmol/L FeSO$_4$.

5.3.3 Electrical properties

Figure 5.4 shows the plots of resistivity for the undoped and Fe-doped samples annealed at different temperatures (the data for the as-deposited film were plotted at 27°C). The resistivity higher than 10^6 Ωcm cannot be measured by our measurement system. Therefore, the electrical resistivity could be higher than 10^6 Ωcm for the as-deposited films and the films annealed at 200 and 300 °C of undoped SnO$_2$. The resistivity was decreased by the 400 °C annealing. The conduction type judged by the hot probe method was n-type for all the samples annealed at 400°C. As is well known, oxygen deficiency is the main reason for the conductivity of undoped SnO$_2$. Therefore, for the undoped film, the nitrogen annealing is thought to increase oxygen vacancies, which act as donors in SnO$_2$, resulting in decrease in

resistivity. For the film deposited using the FeSO$_4$-mixed solution, the resistivity was found to become significantly lower than that of the undoped film after annealing at 300 and 400 °C, as shown in Fig. 5.4. A similar resistivity result was obtained for the film deposited by the separate doping solution containing 20mmol/L FeSO$_4$. However, the resistivity of the film deposited by the separate doping solution containing 200mmol/L FeSO$_4$ is higher than that of the undoped film.
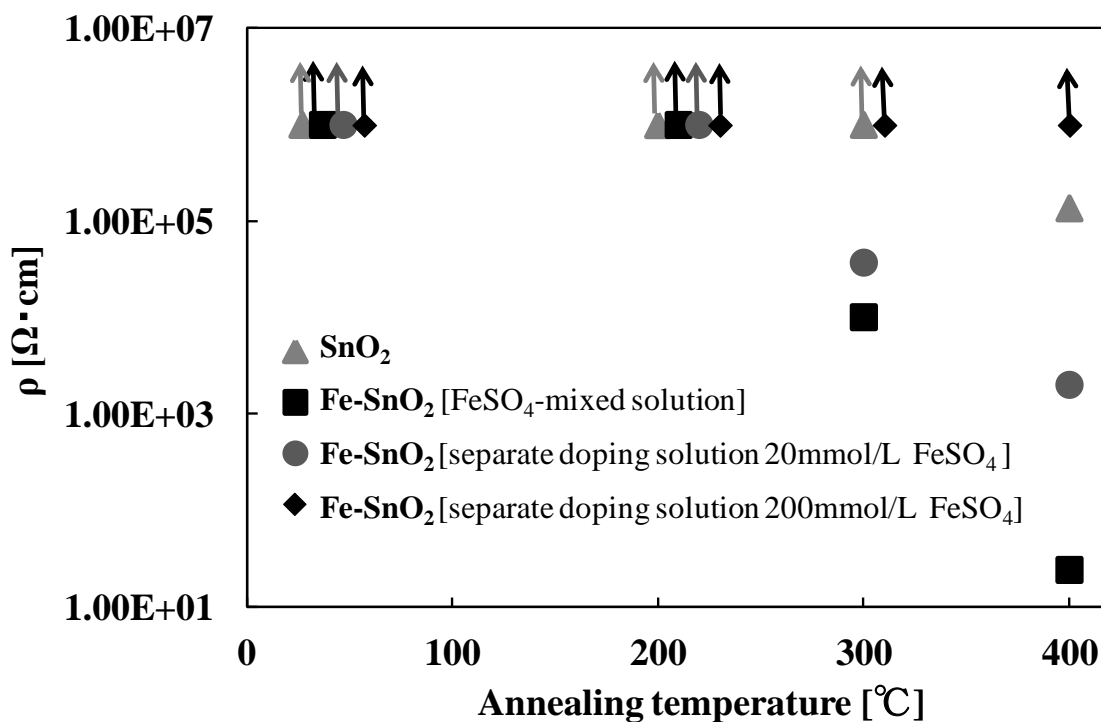
Fig. 5.4 Resistivity of the various SnO$_2$ films annealed at different temperatures.

The morphology of the undoped and Fe-doped SnO$_2$ thin films is shown in Figs. 5.5 (a)-(d). The SEM results reveal that all the SnO$_2$ films have almost the same surface morphology. Consequently, change in the morphology (grain size) is not the main reason why electrical resistivity was reduced by the Fe-doping.

Characterization results of Fe-doped SnO$_2$ films have been reported by a few groups. In ref.9, it was reported that electrical resistivity increases with Fe doping. They considered that

Fe acts as an acceptor in SnO$_2$. Consequently, the compensation of electrons with holes leads to reduction of the overall carrier concentration. The Fe doping also has influence on optical band gap of the SnO$_2$ film. By increasing the doping level, the band gap gradually decreases, which was considered to be related to carrier density reduction (diminish of the Moss-Burstein shift). The similar results have also been reported in ref.7.
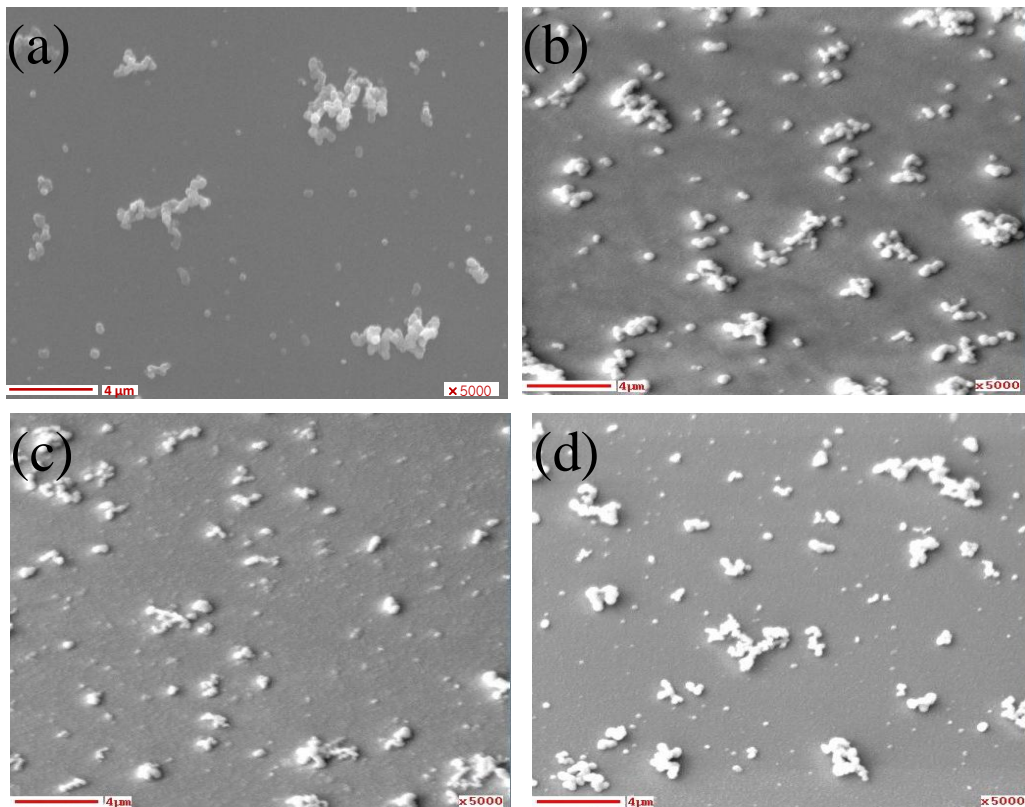
Fig. 5.5 SEM images of the various as-deposited SnO$_2$ films: (a) undoped SnO$_2$, (b) Fe-doped SnO$_2$ deposited with the FeSO$_4$-mixed solution, (c) Fe-doped SnO$_2$ deposited with the separate doping solution containing 20mmol/L FeSO$_4$, (d) Fe-doped SnO$_2$ deposited with the separate doping solution containing 200mmol/L FeSO$_4$.

In our research, the conduction type of the Fe-doped SnO$_2$ thin films is n-type. Therefore, the possible explanation for the resistivity reduction is that some portion of the doped Fe atoms are at interstitial sites and act as a donor. In the chap.4, we indicated that Cu in SnO$_2$ films can occupy an interstitial site and act as a donor. Similarly, the Fe ions at interstitial sites will act as a donor and increase electron concentration. The increase in the resistivity of the

film deposited by separate doping solution containing 200mmol/L FeSO$_4$ could be due to the structural disorder caused by Fe impurity. Another possibility is that when the Fe concentration is high, some portion of Fe atoms occupy a substitutional site and act as an acceptor, leading to compensation of donors. In our results, the band gap was not significantly changed by the Fe doping, as shown in Fig. 5.3. This would be because of the low doping level compared with the previous works [7, 9].

5.4 Conclusion

Fe-doped SnO$_2$ thin films have been deposited on glass substrates using the PCD technique. SnO$_2$-deposition solution is an aqueous solution containing 10 mmol/L SnSO$_4$. For the Fe doping, FeSO$_4$ is mixed in the SnO$_2$ deposition solution, or another solution for the Fe doping is prepared separately and alternately dropped and irradiated. The optical transmission of the film is fairly high in the visible region, and the band gap obtained is 3.8-3.9 eV. The resistivity of the 300 and 400°C annealed films is significantly reduced by the Fe-doping using the 2 mmol/L FeSO$_4$-mixed solution or the separate solution containing 20mmol/L FeSO$_4$. However, the resistivity of Fe-doped SnO$_2$ films deposited with the separate solution containing 200mmol/L FeSO$_4$ is higher than that of undoped films.

References

[1] E. Shanthi, A. Banerjee, V. Dutta, and K. L. Chopra, J. Appl. Phys. 53 (1982) 1615

[2] J. P. Upadhyay, S. R. Vishwakarma, and H. C. Prasad, Thin Solid Films 167 (1988) L7.

[3] J. P. Chatelon, C. Terrier, E. Bernstein, R. Berjoan, and J.A. Roger, Thin Solid Films 247 (1994) 162.

[4] S. Shanthi, C. Subramanian, and P. Ramasamy, J. Cryst. Growth. 197 (1999) 858.

[5] Y. Hu and S. -H. Hou, Mat. Chem. Phys. 86 (2004) 21.

[6] S. Rani, S.C. Roy, and M. C. Bhantnagar, Sens. Actuators B 122 (2007) 204.

[7] T. N. Soitah, C. H. Yang, and L. Sun, Mat. Sci. Semicond. Proc. 13 (2010) 125.

[8] G. Korotcenkova and S. D. Hana, Mat. Chem. Phys. 113 (2009) 756.

[9] M-M. Bagheri-Mohagheghi, N. Shahtahmasebi, M. R. Alinejad, A. Youssefi, and M. Shokooh-Saremi, Solid State Sci. 11 (2009) 233.

[10] M. Muhibbullah and M. Ichimura, Jpn. J. Appl. Phys. 49 (2010) 081102.

Chapter 6

Fabrication of portable hydrogen sensors based on photochemically deposited SnO$_2$ thin films

6.1 Introduction

As described in chap.2, we fabricated highly sensitive room temperature hydrogen sensor based on 200°C annealed nanocrystalline SnO$_2$ thin films by a PCD technique [1-3]. When the sensor is actually employed for detecting hydrogen, the measuring instrument is necessary for reading the electrical signal of the sensor. One drawback of our hydrogen sensor is that since the basic resistance was very high, change of electrical resistance cannot be read by a simple measuring instrument. i.e. the sensor is not compatible with conventional sensor system. In this chapter, in order to control resistance of SnO$_2$ thin film, we attemped high temperature annealing and impurities doping, and the sensor characteristics of the sample were evaluated. Moreover, the portable hydrogen detector was fabricated by combining the sensor with a small measuring instrument that is readily used to measure resistance of a sample.

6.2 Experimental detail

Doped and undoped SnO$_2$ thin films were fabricated by the drop-PCD method. As described in chap. 2, the SnO$_2$ films were deposited by 10-times drop-irradiation cycle. Since SnO$_2$ thin films of comparatively low resistance were obtained by doping Cu and Fe as presented in chap. 4 and chap. 5, Cu and Fe were doped under the following conditions. For the Fe impurity doping, 2 mmol/L FeSO$_4$ was mixed in the SnO$_2$-deposition solution, and the films were deposited by the same drop-irradiation cycles. We obtained a Fe doped SnO$_2$ film with a thickness of about 0.15 μm by repeating the drop-irradiation cycle of 10 times. On the other hand, for the Cu doping, a solution for the SnO$_2$-deposition solution and another

solution for the Cu doping solution including 2 mmol/L $CuSO_4$ were prepared separately. A small amount of each of these solutions was alternately dropped on the glass substrate, and irradiated by the UV light. We repeated the drop-irradiation cycles 20 times (10 times for the SnO_2 deposition and 10 times for the doping, alternately) and obtained Cu doped SnO_2 thin films with a thickness of around 0.15 μm. To enhance sensitivity to hydrogen, Pd was doped by a similar photochemical technique. A 2mmol/L $PdCl_2$ solution was dropped onto the SnO_2 film surface, and then irradiated with the UV light for 5 min. And vapor deposition of Au electrodes was performed. The samples were annealed in nitrogen ambient at 400°C.

The gas sensor characteristic is evaluated as described in chap. 2. The sample was put on the stage (with its temperature adjusted at 300K) of the test chamber, the current at an applied voltage of 2V was measured, first in vacuum (about 50 Pa), and then in 5% H_2+Ar mixed gas (0.1atm) ambient.
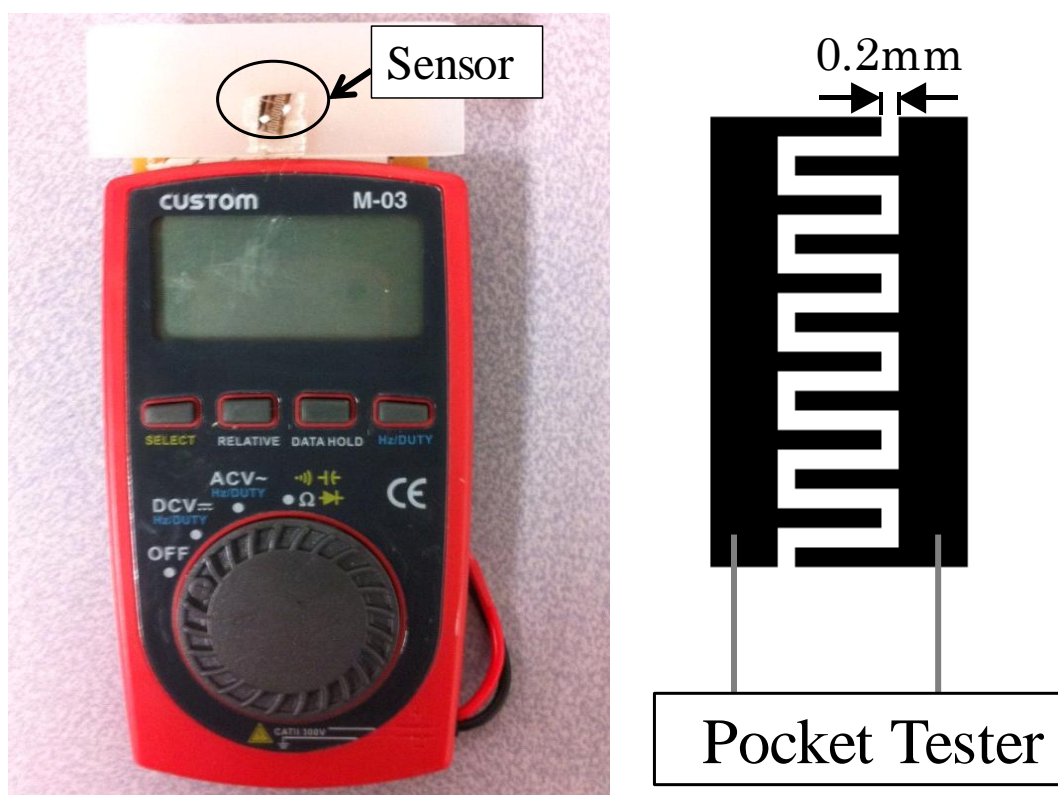

Fig. 6.1 The portable detector.

Furthermore, two leads of the pocket tester were connected with two electrodes of the sample with the gold wire, and the portable hydrogen detector was fabricated. The appearance is shown in Fig. 6.1. To examine the sensing property of the detector, the portable detector was put on the test chamber, 0.1atm Ar+H$_2$ mixed gas was introduced by the same method as mentioned above, and then the resistance change was measured. Moreover, influence of the air cannot be neglected in employment of an actual hydrogen gas detector. Therefore, 0.8 atm air was first introduced and 0.1atm hydrogen was introduced. Then the resistance change was measured.

6.3 Results and discussion

6.3.1 Sensor characteristics

6.3.1.1 Response properties

Doped and undoped 400°C annealed SnO$_2$ thin film sensors were fabricated by the above-mentioned process, and the response to 5% H$_2$+Ar (0.1atm) of each sample was shown in Fig. 6.2. At the time of 15 minutes after exposure in hydrogen, the change in resistance of each sample is 1.2×10^3, 2.3×10^4, and 7.3×10^4 for undoped, Cu and Fe doped SnO$_2$ sample, respectively. The change in resistance of the Cu and Fe doped films is much higher than that of undoped SnO$_2$. Thus, the sensitivity is increased by Cu and Fe doping. For n-type oxide semiconductors, an oxygen atom adsorbed on the surface traps some of the carriers to become a negative ion at the grain boundary. These adsorbed oxygen ions generate a potential barrier between grains, which must disturb the free conduction of the electrons. Under the hydrogen ambient, the oxygen ions are removed by reactions with hydrogen atoms, which leads to decrease in the barrier height and decrease in the resistance. The present results indicate that in this process, the doped Fe and Cu work as a catalyst like Pd and consequently enhance the sensitivity. For the portable detector fabrication and evaluation described in the next section,

we used the Fe doped and undoped SnO$_2$ sample since the Fe doped sensor exhibits better response characteristics than the Cu doped sensor.
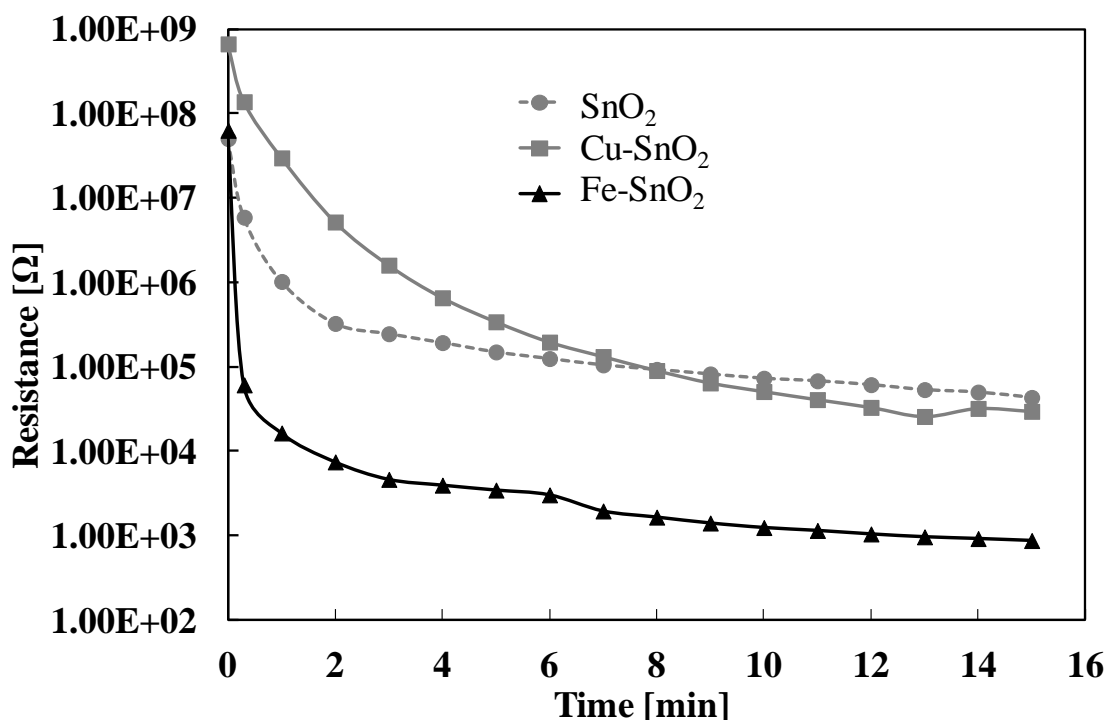

Fig. 6.2   Response to the 5% H$_2$+Ar mixed gas (0.1atm) of various sample.

6.3.1.2 Recovery properties

The recovery characteristics are also important characteristics of a gas sensor. The sensor resistance which is decreased with introduction of hydrogen should increase when hydrogen is removed. Figures 6.3 and 6.4 shows the recovery characteristics of the undoped and Fe doped sample annealed at 400°C. First the sensor response was measured on the same conditions as above in hydrogen. Next the chamber was vacuumed at 15 minutes after exposure in hydrogen, and then air was introduced up to 1.0atm. The result shows that the resistance of the undoped sample increased by 3 orders of magnitude almost instantly when exposed in the air. The result was comparable to that of the 200°C annealed SnO$_2$ sample reported in chap. 2. However, the resistance of Fe doped sample increased only by 2 orders of

magnitude within 15 minutes when exposed in the air as shown in Fig. 6.4. The sensitivity is almost the same for 200°C annealed SnO$_2$ and 400°C annealed Fe doped SnO$_2$ sample. However, the recovery speed is significantly different. The detailed reason has not become clear yet.

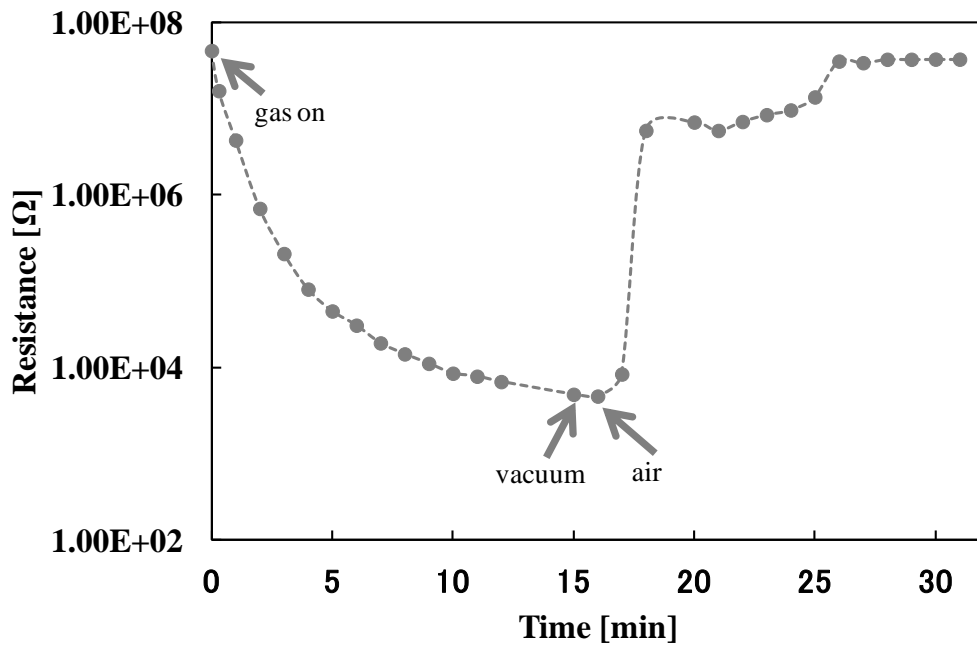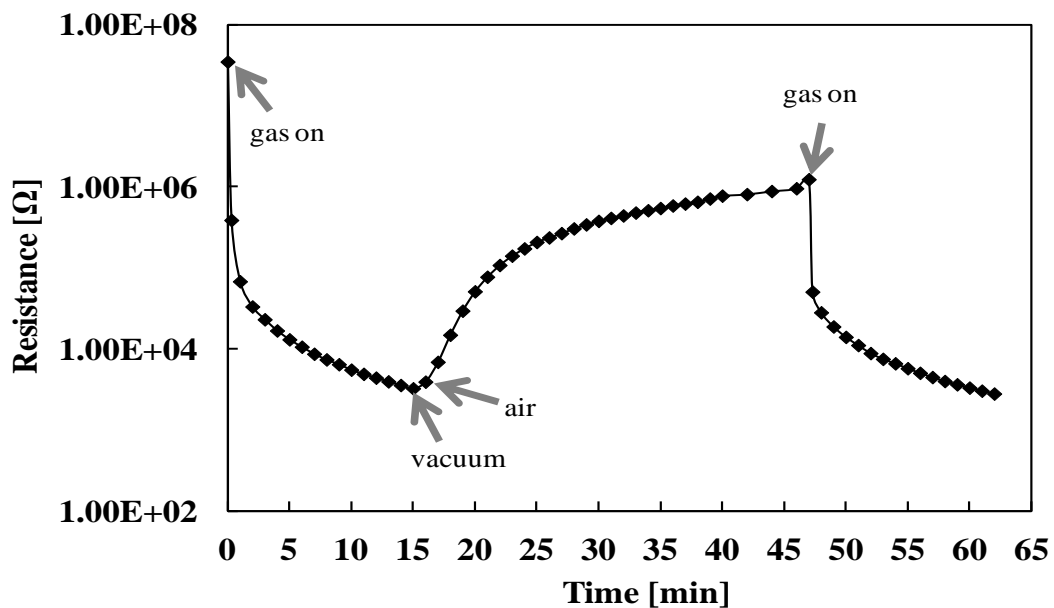**Fig. 6.3 Recovery characteristics of the undoped SnO$_2$.**

Fig. 6.4 Recovery characteristics of the Fe doped SnO$_2$.

71

6.3.2 Investigation of potable hydrogen detector

To examine the sensing property of the portable detector, the response to 5% H$_2$+Ar (0.1atm) of various samples was investigated by the same method as above. The results are shown in Fig. 6.5. While the resistance before introduction hydrogen of the undoped 200°C annealed SnO$_2$ sample was $10^{10} \sim 10^{11}\Omega$, the resistance before introduction of hydrogen of the 400°C annealed sample was about $10^6\Omega$ as shown in 0 (min) data of Fig. 6.5. Thus the resistance decreased notably by high temperature annealing. When these samples were exposed to hydrogen, the change in resistance of the Fe doped film is larger than that of the undoped SnO$_2$ by almost one order of magnitude.
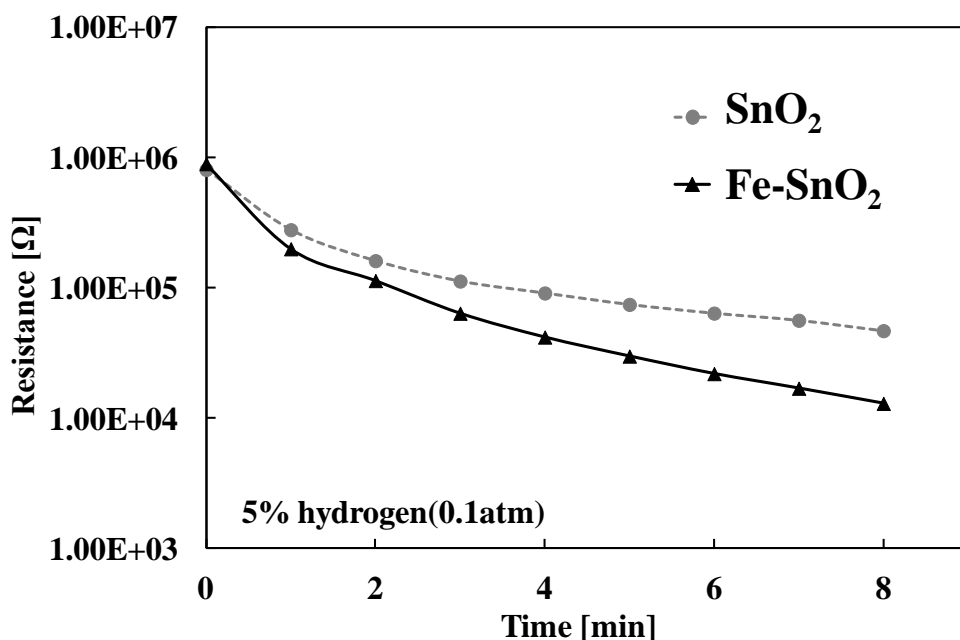

Fig. 6.5 Response of the undoped and Fe-doped SnO$_2$ detectors.

Since the sensor needs to detect hydrogen in air in the actual application, we investigate effects of air on the sensor response. 0.8 atm air was first introduced, and then 0.1atm hydrogen was introduced into the test chamber and the resistance change was measured. The

results are shown in Fig.6.6. For the Fe doped SnO_2 sample, two orders of magnitude reduction of resistance was observed by introduction of hydrogen into air. The change in resistance of Fe doped SnO_2 is much higher than undoped SnO_2, which is the same results as in the case that only hydrogen is introduced in the chamber. On the other hand, the speed of response was slower compared with the case of only hydrogen introduction. Upon exposure to hydrogen, the fixed charge of O^- will be removed by the following reaction.

$$H_2 + O^- = H_2O + e^- \qquad\qquad (1)$$

In the case of the mixed gas of the air and hydrogen, both O_2 and H_2O in air can increase the amount of O^-, thereby slowing down the resistance decrease upon the exposure to hydrogen [3].
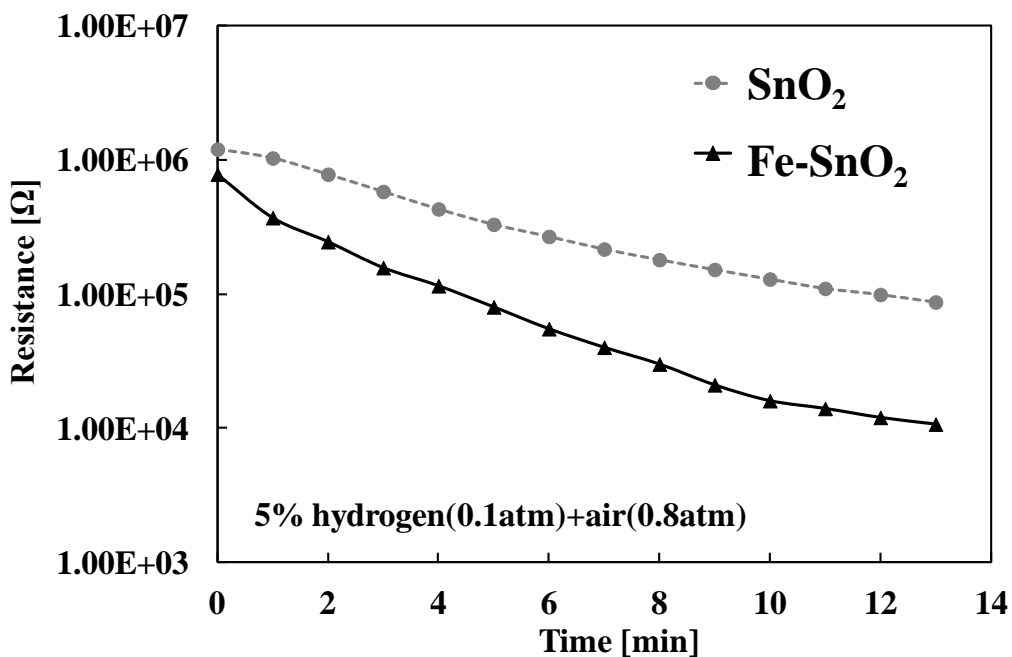

Fig. 6.6 Response of the undoped and Fe-doped SnO₂ detectors.

6.4 Conclusion

We fabricated room temperature portable hydrogen sensors based on doped and undoped SnO_2 films. The films were deposited by the PCD and annealed at 400°C. The doped and undoped

samples showed resistance decrease by a factor $>10^3$ for a 5% H_2+Ar mixed gas (0.1atm) at room temperature. Furthermore, by combining the sample with a pocket tester, we fabricated the portable type hydrogen detector, and the response was investigated. The Fe doped SnO_2 detector showed comparatively high sensitivity to the mixed gas of the air and hydrogen. Therefore, it can be employed for a wide range of applications for safety and efficient operation of a fuel cell system.

References

[1] D. Ito, and M. Ichimura, Jpn. J. Appl. Phys. 45 (2006) 7094.

[2] M. Ichimura, and T. Sueyoshi, Jpn. J. Appl. Phys. 48 (2009) 015503.

[3] M. Ichimura, Aodengbaoleer, and T. Sueyoshi, Phys. Status Solidi C 7 (2010) 1168.

Chapter 7

Conclusions

7.1 Main conclusions of this work

Highly sensitive room temperature hydrogen sensors based on SnO_2 films were fabricated and characterized. SnO_2 thin films have been deposited from aqueous solution containing $SnSO_4$ by the drop-photochemical deposition technique. A solution were dropped onto the glass substrate and irradiated with UV light of an ultra-high-pressure mercury arc-lamp. After 5 min irradiation, the substrate was washed and the new solution was dropped. The films were fabricated by repeating this process. To enhance the sensitivity for hydrogen, Pd was doped by a similar photochemical technique. A solution containing Pd^{2+} ions was dropped on the SnO_2 film surface and irradiated with UV light. The sample annealed at 200 °C showed current increase by a factor $>10^4$ within 1 min for 5% H_2+Ar mixed gas (0.1atm) at room temperature. The removal of hydrogen from the ambient caused only a small decrease in the current, but the current decreased by more than three orders of magnitude almost instantly upon subsequent exposure to air.

The effect of UV irradiation on hydrogen sensors based on photochemically deposited SnO_2 thin films was studied in detail. The 200°C annealed samples were irradiated with UV light using a low-pressure mercury lamp in vacuum and in air for one hour. The sensitivity and response speed were further improved by UV irradiation. The detailed XPS results revealed that the percentages of metal Pd, PdO and PdO_2 were almost the same for the no irradiation sample and UV irradiated sample, and Pd was dominantly in the metallic or elemental state. Therefore, the sensitivity improvement by the UV irradiation is not only due to change in the chemical states of Pd atoms but also other factors such as rearrangement of Sn-O bonding and incorporation of impurity atoms.

Sb-doped and Cu-doped SnO_2 thin films have been deposited on glass substrates using the photochemical deposition technique. A solution containing $SnSO_4$ and a doping solution containing $SbCl_3$ or $CuSO_4$ were alternately dropped on the glass substrate and irradiated by the UV light. The Auger electron spectroscopy measurement revealed that Sb or Cu is contained in the deposited thin films. The Sb/Sn atomic ratio in the film is as high as 0.53. In contrast, the Cu/Sn atomic ratio is relatively low, around 0.1. The optical transmission of the film is fairly high in the visible region, and the band gap obtained is 3.7 - 3.8 eV. The resistivity of the 400°C annealed films is significantly lower for the Cu-doped film than for the undoped and Sb-doped films. The Hall measurement results showed that the electron concentration is 3×10^{16} cm^{-3} for the Cu-doped SnO_2 films annealed at 400°C.

Fe-doped SnO_2 thin films have been deposited on glass substrates using the photochemical deposition technique. SnO_2-deposition solution was an aqueous solution containing 10 mmol/L $SnSO_4$. For the Fe doping, $FeSO_4$ was mixed in the SnO_2 deposition solution, or another solution for the Fe doping was prepared separately and alternately dropped and irradiated. The Auger electron spectroscopy measurement revealed that Fe was contained in the deposited thin films when the separate solution was used. The Fe/Sn atomic ratios are about 0.07 and 0.11 with the doping solution containing 20 and 200 mmol/L $FeSO_4$, respectively. The optical transmission of the film is fairly high in the visible region, and the band gap obtained is 3.8-3.9 eV. The resistivity of the 300 and 400°C annealed films is significantly reduced by the Fe-doping using the 2 mmol/L $FeSO_4$-mixed solution and the separate solution containing 20mmol/L $FeSO_4$. However, the resistivity of Fe-doped SnO_2 films deposited with the separate solution containing 200mmol/L $FeSO_4$ is higher than that of undoped films.

Highly sensitive room temperature hydrogen sensors based on the doped and undoped SnO_2 films were fabricated by the photochemical deposition and annealing at 400°C. The doped and undoped samples showed resistance decrease by a factor $>10^3$ for a 5% H_2+Ar mixed gas (0.1atm) at room temperature. Furthermore, by combining the sample with a

pocket tester, we fabricated the portable type hydrogen detector, and the response was investigated. The Fe doped SnO_2 detector show comparatively high sensitivity to the mixed gas of the air and hydrogen. Therefore, it can be employed for a wide range of applications for safety and efficient operation of a fuel cell system.

7.2 Suggestions for future work

In the present work, high sensitivity room temperature hydrogen sensors were fabricated by the photochemical method. However, the detailed mechanism of the high sensitivity are not understood clearly. The resistivity is considered to be dominantly controlled by barriers at the grain boundaries. Therefore, we suggest microscopic measurement of change in a surface potential distribution upon introduction of gas by a scanning probe microscopy, in order to clarify relationship between the potential barrier and the gas ambient.

Antimony Sb was successfully doped into SnO_2 thin films by drop-photochemical technique. Howerver, the Sb atoms did not replace Sn atoms but formed a separate high resistivity phase, probably Sb_2O_3. Therefore, for doping of Sb into the substitutional sites, we suggest use of a much more diluted $SbCl_3$ doping solution.

Since we established the doping technique in photochemical deposition of SnO_2, any other elements such as Al and Zn can be chosen as dopants for SnO_2. Those elements have been used to obtain p-type SnO_2, and they also can influence structural, morphological, optical and electrical properties. Fabrication and characterization of the sensor based on SnO_2 thin films doped with those elements are also suggested.

At present, various metal oxide semiconductors have been widely used for sensor. So far we have employed the photochemical deposition technique to deposit SnO_2 thin films and applied them to sensors. However, photochemical deposition of other oxide materials has not been tried. We expected that other oxide materials deposited by photochemical deposition are

also formed of nanoparticles and can be applicable for a high sensitivity sensor. If the sensitivity strongly depends on materials, the sensing mechanism may be elucidated by analyzing the difference between materials. Therefore, it should be interesting to attempt to synthesize other oxide materials such as ZnO and WO_{3-x} by the photochemical deposition technique and apply them to sensors.

Journals

1) M. Ichimura, Aodeng Baoleer, T. Sueyoshi, "Properties of gas sensors based on photochemically deposited nanocrystalline SnO_2 films", Phys. Status Solidi C. 7 (2010) 1168.

2) Dengbaoleer Ao, Masaya Ichimura, "UV irradiation effects on hydrogen sensors based on SnO_2 thin films fabricated by the photochemical deposition", Solid-State. Electron. 69 (2012) 1.

3) Dengbaoleer Ao, Masaya Ichimura, "Deposition and characterization of Sb and Cu doped nanocrystalline SnO_2 thin films fabricated by the photochemical method" J. Non-Cryst. Solids 358 (2012) 2470.

4) Dengbaoleer Ao, Masaya Ichimura, "Deposition of Fe doped nanocrystalline SnO_2 thin films by the photochemical deposition method" Trans. Mater. Res. Soc. Jpn. 37 (2012) 377.

5) オ ドンボリル，森口幸久，市村正也，"光化学堆積 SnO_2 薄膜を用いた携帯式水素検出器の試作" 電気学会論文誌 A（基礎・材料・共通部門誌）133 (2013)
（ Dengbaoleer Ao, Yukihisa Moriguchi, Masaya Ichimura, "Fabrication of portable hydrogen detectors based on photochemically deposited SnO_2 thin films", IEEJ Trans. Fundamentals and Materials. in press 133 (2013))

Presentations

1) Dengbaoleer Ao, Masaya Ichimura:

"UV irradiation effects on hydrogen sensors based on SnO_2 thin films fabricated by the photochemical deposition"

Renewable Energy 2010, June 27 - July 2, 2010, Yokohama, Japan.

2) Dengbaoleer Ao, Masaya Ichimura:

"Deposition and characterization of Sb and Cu doped nanocrystalline SnO_2 thin films fabricated by the photochemical method"

24th International Conference on Amorphous Nanocrystalline Semiconductor, August 21-26, 2011, Nara Japan.

3) Dengbaoleer Ao, Masaya Ichimura:

"Deposition of Fe doped nanocrystalline SnO_2 thin films by the photochemical deposition method"

21st Academic Symposium of MRS-Japan 2011, December 19-21, 2011, Yokohama, Japan.

4) Dengbaoleer Ao, Yukihisa Moriguchi, Masaya Ichimura

"Fabrication of portable hydrogen detectors based on photochemically deposited SnO_2 thin films"

The Institute of Electronics, Information and Communication Engineers Technical Meeting, May 16, 2012, Toyohashi, Japan.

5) Dengbaoleer Ao, Yukihisa Moriguchi, Masaya Ichimura

"Fabrication of portable hydrogen detectors based on photochemically deposited SnO_2 thin films"

73th Autumn Meeting, The Japan Society of Applied Physics, September 11-14, 2012, Ehime, Japan.